Deciphering the influence of evolutionary legacy and functional constraints on the patella: an example in modern rhinoceroses amongst perissodactyls

Christophe Mallet[1,2] and Alexandra Houssaye[3]

[1] Faculty of Engineering, University of Mons, Department of Geology and Applied Geology, Mons, Belgium
[2] Institute of Natural Sciences, Operational Directorate Earth and History of Life, Brussels, Belgium
[3] Muséum National d'Histoire Naturelle, Mécanismes adaptatifs et évolution (MECADEV), UMR 7179, MNHN, CNRS, Paris, France

ABSTRACT

In mammals, the patella is the biggest sesamoid bone of the skeleton and is of crucial importance in posture and locomotion, ensuring the role of a pulley for leg extensors while protecting and stabilizing the knee joint. Despite its central biomechanical role, the relation between the shape of the patella and functional factors, such as body mass or locomotor habit, in the light of evolutionary legacy are poorly known. Here, we propose a morphofunctional investigation of the shape variation of the patella among modern rhinoceroses and more generally among perissodactyls, this order of ungulates displaying a broad range of body plan, body mass and locomotor habits, to understand how the shape of this sesamoid bone varies between species and relatively to these functional factors. Our investigation, relying on three dimensional geometric morphometrics and comparative analyses, reveals that, within Rhinocerotidae and between the three perissodactyl families, the shape of the patella strongly follows the phylogenetic affinities rather than variations in body mass. The patellar shape is more conservative than initially expected both within and between rhinoceroses, equids and tapirs. The development of a medial angle, engendering a strong mediolateral asymmetry of the patella, appears convergent in rhinoceroses and equids, while tapirs retain a symmetric bone close to the plesiomorphic condition of the order. This asymmetric patella is likely associated with the presence of a "knee locking" mechanism in both equids and rhinos. The emergence of this condition may be related to a shared locomotor habit (transverse gallop) in both groups. Our investigation underlines unexcepted evolutionary constraints on the shape of a sesamoid bone usually considered as mostly driven by functional factors.

INTRODUCTION

In vertebrates, the shape of the skeleton is strongly influenced by structural, functional, developmental constraints, and evolutionary legacy (*Seilacher, 1970*, *1991*; *Gould, 2002*).

Limb bones, which function in like body support and locomotion in quadrupeds, are particularly influenced by functional constraints (*Hildebrand, 1974*; *Hall, 2007*). Variations of body plan, body mass or locomotor habits induce changes in the shape of limb elements (*Hildebrand, 1974*; *Polly, 2007*; *Biewener & Patek, 2018*), as observed in many clades of tetrapods (see for example *Fabre et al., 2013*; *MacLaren & Nauwelaerts, 2016*; *Etienne et al., 2020a*; *Serio, Raia & Meloro, 2020*). However, despite this intense exploration of form-function relationships focused mainly on limb long bones, smaller elements like sesamoid bones remain poorly studied. Sesamoids are small concentrations of bone generally embedded in dense connective tissue such as tendons or ligaments. They are assumed to increase leverage for muscles and tendons attached to them, while protecting the joints with which they are associated (*Vickaryous & Olson, 2008*). The emergence of sesamoids in some joints is directly linked to variations in mechanical loads, making them likely to carry a strong functional signal (*Vickaryous & Olson, 2008*; *Eyal et al., 2019*).

The patella is the largest sesamoid bone of the skeleton (*Samuels, Regnault & Hutchinson, 2017*). Long considered to form within the distal quadriceps tendon, recent findings show that the patella arises as a bony process at the anterodistal surface of the femur (*Eyal et al., 2015*, *2019*). The patella is later embedded into the quadriceps tendon and articulates with the femur by sliding onto the distal trochlear groove. Onto the patella attach the different ends of the *musculus quadriceps* as well as the *m. gluteobiceps*, all being knee extensors (*Barone, 2010a*; *Samuels, Regnault & Hutchinson, 2017*; *Etienne, Houssaye & Hutchinson, 2021*) (Fig. 1). The patella is also connected to the tibia through the patellar tendon, and additional lateral and medial tendons (*Barone, 2010a*; *Samuels, Regnault & Hutchinson, 2017*). The main functional role of the patella is to modify the lever arm of the *m. quadriceps*. By moving the quadriceps tendon away from the centre of rotation of the knee joint, the patella acts as a pulley and reduces the muscular energy required to extend the leg, while increasing the velocity of the rotation (*Aglietti & Menchetti, 1995*; *Allen et al., 2017*). In mammals, the patella also centralizes the forces coming from the four heads of the *m. quadriceps* into a single point of application and transmits them without friction to the tibial tuberosity. In addition, the patella acts as a protective element for the knee joint (*Aglietti & Menchetti, 1995*).

The functional importance of the patella led to various works that explored the biomechanical involvement of this sesamoid bone in the hindlimb movements and its mechanical advantage, mostly in humans and related hominoids (*Bizarro, 1921*; *Ellis et al., 1980*; *Aglietti & Menchetti, 1995*; *Lovejoy, 2007*; *Dan et al., 2018*; *Pina et al., 2020*; *Schneider, Rooks & Besier, 2022*). These aspects have been rarely addressed in other groups of amniotes (*Alexander & Dimery, 1985*; *Chadwick et al., 2014*; *Allen et al., 2017*), most of the studies focusing more on the evolutionary relevance of the presence or absence of the patella (*Jerez, Mangione & Abdala, 2010*; *Ponssa, Goldberg & Abdala, 2010*; *Corina Vera, Laura Ponssa & Abdala, 2015*; *Abdala, Vera & Ponssa, 2017*; *Samuels, Regnault & Hutchinson, 2017*). While the inner bony structure of the patella has sometimes been explored in regards to functional constraints (*Raux et al., 1975*; *Toumi et al., 2006*; *Houssaye, de Perthuis & Houée, 2021*), the variation of its external shape, considered as relatively conservative in amniotes (*Samuels, Regnault & Hutchinson, 2017*), remains
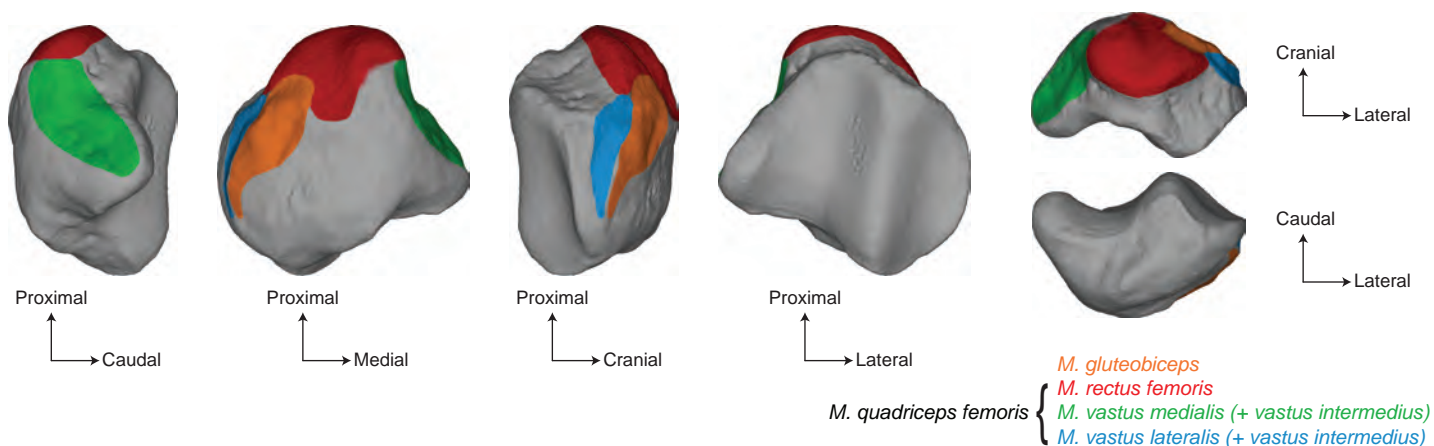
M. quadriceps femoris {
M. gluteobiceps
M. rectus femoris
M. vastus medialis (+ vastus intermedius)
M. vastus lateralis (+ vastus intermedius)

Figure 1 **Main muscular insertions on the patella of a white rhinoceros (*Ceratotherium simum*).** Muscle insertions replaced on the 3D model of *Ceratotherium simum cottoni* AMNH M-51854 based on the anatomical descriptions of *Barone (2010a)* and *Etienne, Houssaye & Hutchinson (2021)*.
Full-size 🖼 DOI: 10.7717/peerj.18067/fig-1

largely understudied. Only a few studies tried to investigate the form-function relationships at a larger interspecific scale, mostly in mammals (*Valois, 1917*; *Raymond & Prothero, 2012*; *Pina et al., 2020*; *Garnoeva, 2022*). Therefore, the variation of the shape of the patella in relation with functional constraints remains virtually unknown in amniotes.

In this context, we chose to explore the shape variation of the patella in modern rhinoceroses and compare it with shape variation within perissodactyls (adding equids and tapirs) to investigate its relations with functional factors within a phylogenetically informed framework. Modern rhinoceroses constitute the second heaviest land mammal group after elephants (*Alexander & Pond, 1992*), and contrary to them, show great variations (factor of 6) of body mass (BM) among the five living species: from 600 kg for *Dicerorhinus sumatrensis* (*Fischer, 1814*) up to 3,500 kg for *Ceratotherium simum* (*Burchell, 1817*). These three-toed animals inhabit various environments from open savannas to dense rainforests, associated with diverse feeding strategies, from specialized grazers to generalist browsers (*Dinerstein, 2011*). They perform transverse gallop (*Economou et al., 2020*) and are able to reach speeds from 27 km.h^{-1} for *Ceratotherium simum* to 45 km.h^{-1} for *Diceros bicornis* (*Garland, 1983*; *Alexander & Pond, 1992*; *Blanco, Gambini & Fariña, 2003*). Body mass in rhinos can vary strongly between males and females in some species (*Zschokke & Baur, 2002*; *Dinerstein, 2011*), as well as their body plan, from long-legged black rhino *Diceros bicornis* to short-legged white rhino *C. simum*. This diversity of body construction and ecological preferences makes them a particularly well-suited group for studying the link between patellar shape and functional factors.

To expand the scope of our investigation, we chose to include in a second time other modern perissodactyls as comparative groups. The other modern perissodactyls comprise seven species of equids and four of tapirs. These two clades show less intragroup variations of size and body plan. Tapirs are forest-dwellers with a limited range of body mass (factor of 2): from 175 to 400 kg (*Medici, 2011*). Tapirs retain some plesiomorphic characters of the order Perissodactyla in their limbs, such as a tetradactyl manus and a tridactyl pes

(*MacLaren & Nauwelaerts, 2016*, *2017*). Their running pace is different from that of rhinos, as they perform a rotary gallop (*Economou et al., 2020*). As for equids, they show marked weigh variations related to domestication, although not comparable to what is observed among rhinos. If most wild equids weigh around 300 kg, some domestic horses and donkeys (such as draft races) can exceed 800 kg (factor of 2.6). In addition, equids show a highly derived limb structure adapted for running and living in open habitats, with monodactyl manus and pes (*Rubenstein, 2011*), associated with a transverse gallop as for rhinos (*Economou et al., 2020*). These three families (Rhinocerotidae, Tapiridae, Equidae) also show a gradient of stature and proportions in their limb construction, from cursorial equids to "mediportal" tapirs and "graviportal" rhinos, likely to be associated with differences in patellar shape (*Eisenmann & Guérin, 1984*). Recent advances in functional morphology underlined how body mass could drive–or not–the shape of limb bones in perissodactyls (*MacLaren & Nauwelaerts, 2016*, *2017*; *Hanot et al., 2017*, *2018*; *MacLaren et al., 2018*; *Mallet et al., 2019*, *2020*, *2021*, *2022*; *Etienne et al., 2020b*), but without consideration for the patella.

Moreover, rhinoceroses and equids are known to possess a "knee locking" mechanism in their hindlimb: they are able to lock the patella and the medial patellar tendon above the medial trochlear ridge of the distal femur (*Hermanson & MacFadden, 1996*; *Schuurman, Kersten & Weijs, 2003*). Doing so, the natural flexion of the limb that could be engendered in relation with body weight becomes impossible, allowing these animals to save muscular energy for long periods of standing. Long considered as passive, *in vivo* experiments demonstrated that this mechanism does require muscular energy, even though far much less than would be needed without this apparatus (*Schuurman, Kersten & Weijs, 2003*). Broadly studied in domestic equids for veterinary purposes, this locking mechanism is less documented *in vivo* in rhinos and only inferred through the shape of the distal femur but not directly through that of the patella (*Shockey et al., 2008*; *Danaher, Shockey & Mihlbachler, 2009*; *Janis et al., 2012*; *Mihlbachler et al., 2014*). A recent investigation on the microanatomy of the patella in modern perissodactyls highlighted microanatomical changes related to different functional factors, notably the presence of the knee locking mechanism (*Houssaye, de Perthuis & Houée, 2021*). But a similar comparative investigation remains to be conducted for deciphering how functional factors are related to the external shape of the patella in this group.

For all these reasons, we chose to explore both intra- and interspecific variation of the shape of the patella among modern rhinoceroses, and to compare it with tapirs' and equids', to shed light on how this crucial sesamoid bone is influenced by functional constraints (body mass, locomotor habit, presence or not of a "knee locking" mechanism) and evolutionary legacy among Perissodactyla. We relied on a 3D geometric morphometrics approach to investigate the form-function relationships on the patella. Given previous results on the shape variation of hindlimb long bones (*Mallet et al., 2019*, *2020*) and on the inner structure of the patella (*Houssaye, de Perthuis & Houée, 2021*) in modern rhinos, we hypothesize: (1) higher interspecific than intraspecific variation of the shape of the patella in rhinos; (2) a patellar morphology not explained by phylogenetic

relations alone but also by functional factors such as body mass, presence or absence of a knee locking mechanism, and type of gallop in perissodactyls (*Schuurman, Kersten & Weijs, 2003*; *Shockey et al., 2008*; *Economou et al., 2020*). The consideration of equids and tapirs will allow us to situate the variation observed among rhinoceroses within the perissodactyls as a whole, and see whether the trends observed, and the hypotheses of functional links highlighted in rhinoceroses are confirmed by this contextualization on the scale of the whole family, or whether different trends between families could call into question the suggested links between form and function.

MATERIALS AND METHODS

Studied sample

We selected a sample composed of 54 patellae of modern perissodactyls housed in eight institutions (American Museum of Natural History, New York, USA; Powell Cotton Museum, Birchington-on-Sea, UK; Idaho Museum of Natural History, Pocatello, USA; Muséum National d'Histoire Naturelle, Paris, France; Museum of Vertebrate Zoology, Berkeley, USA; Natural History Museum, London, UK; Naturhistorisches Museum Basel, Basel, Switzerland; Institute of Natural Sciences, Brussels, Belgium) and representing the five modern species of rhinos (27 patellae), together with four modern species of tapirs (12 patellae) and seven species (nine subspecies) of modern equids (15 patellae) (Table 1, Fig. 2). We used binomial names as provided in the Handbook of Mammals of the World (vol. 2) (*Dinerstein, 2011*; *Medici, 2011*; *Rubenstein, 2011*). The sample includes 29 males, 17 females and 19 specimens without sex attribution. It involves only adult specimens (*e.g.*, having fully fused epiphysis on the long bones associated with the patella), except for one specimen of unclear age but showing a general adult aspect and size and one *Equus zebra hartmannae* considered as subadult (*e.g.*, having not fully fused epiphysis on the associated long bones) (see Table 1 for details). This last one has been kept in the sample as it was the only available specimen we encountered for this subspecies. Because of the higher intrafamilial diversity of rhinos, we chose to focus first on this group. We performed our analyses successively on rhinoceroses only, then on rhinos, equids, and tapirs together. Exploration of shape variation among equids and tapirs respectively are provided as Supplemental Data. All anatomical terms follow classic anatomical and veterinary works (*Federative Committee on Anatomical Terminology, 1998*; *Barone, 2010b*), and are given in Fig. 3.

3D models

Twenty-four patellae were digitized using a structured-light three dimensional scanner (Artec Eva) and reconstructed with Artec Studio professional (v12.1.1.12; Artec 3D, Luxembourg, Belgium). Twelve specimens were scanned using a Creaform HandySCAN 300 laser surface scanner and reconstructed using the VX Models software (Creaform, Houston, TX, USA). Fifteen patellae were scanned using high-resolution computed tomography at the micro-CT laboratory of the Natural History Museum, London, UK (Nikon HMX 225 ST system), and six at the AST-RX platform at the Muséum National

Table 1 List of the studied specimens with family, genus and species names, mean body mass, institutions, sex, age class, condition, and 3D acquisition details.

Family	Taxon	Mean body mass (kg)	Institution	Collection number	Sex	Age	Condition	3D acquisition
Rhinocerotidae	*Ceratotherium simum*	2,300	AMNH	M-51854	F	A	W	SL
			AMNH	M-51855	M	A	W	SL
			AMNH	M-51857	F	A	W	SL
			AMNH	M-51858	M	A	W	SL
			AMNH	M-81815	U	A	U	SL
			BICPC	NH.CON.37	F	A	W	SL
			BICPC	NH.CON.110	M	A	W	SL
			BICPC	NH.CON.112	M	A	W	SL
			MNHN	ZM-MO-2005-297	M	A	C	CT
			NHMUK	ZD 2018.143	U	A	U	SL
	Diceros bicornis	1,050	AMNH	M-113777	U	A	W	SL
			MNHN	ZM-AC-1944-278	M	A	C	CT
			NHMUK	ZD 1879.9.26.6	U	U	U	CT
	Dicerorhinus sumatrensis	775	AMNH	M-81892	M	A	W	SL
			NHMUK	ZD 1879.6.14.2	M	A	W	SL
			NHMUK	ZD 1894.9.24.1	U	A	W	SL
			NHMUK	ZE 1948.12.20.1	U	A	U	SL
			NHMUK	ZE 1949.1.11.1	U	A	W	SL
			NHMUK	ZD 2004.23	U	A	W	SL
	Rhinoceros sondaicus	1,350	MNHN	ZM-AC-A7970	U	A	U	SL
			NHMUK	ZD 1871.12.29.7	M	A	W	SL
	Rhinoceros unicornis	2,000	AMNH	M-35759	M	A	C	SL
			AMNH	M-54454	F	A	W	SL
			MNHN	ZM-AC-1967-101	F	A	C	SL
			NHMUK	ZE 1961.5.10.1	M	A	W	SL
			NHMUK	ZD 1972.822	U	A	U	SL
			NHMUK	ZD 1884.12.1.2	F	A	W	SL
Tapiridae	*Tapirus bairdii*	260	MVZ	141172	U	A	U	LS*
	Tapirus indicus	340	MNHN	ZM-AC-1931-528	M	A	C	CT
			MNHN	ZM-AC-1945-460	M	A	C	CT
			NMB	8125	F	A	C	CT
			RBINS	1184D	M	A	C	LS
			RBINS	1184E	M	A	C	LS
	Tapirus pinchaque	175	MNHN	ZM-AC-1982-34	M	A	C	CT
			MNHN	ZM-AC-1877-765	U	A	U	CT
	Tapirus terrestris	220	MNHN	ZM-AC-1937-1	U	A	C	CT
			MNHN	ZM-MO-1990-20	M	A	C	CT
			RBINS	1185D	M	A	C	LS
			RBINS	1185E	U	A	C	LS

Table 1 (continued)

Family	Taxon	Mean body mass (kg)	Institution	Collection number	Sex	Age	Condition	3D acquisition
Equidae	*Equus africanus asinus*	275	MNHN	ZM-AC-1893-634	M	A	C	CT
			MNHN	ZM-2005-717	U	A	U	CT
			RBINS	12970	F	A	C	LS
			RBINS	13076	F	A	C	LS
	Equus hemionus	230	MNHN	ZM-AC-1880-1103	M	A	C	CT
	Equus ferus caballus	490	MNHN	ZM-AC-A541	F	A	C	CT
			MVZ	162289	M	A	C	LS*
	Equus ferus przewalskii	250	MNHN	ZM-AC-1975-124	F	A	C	CT
			RBINS	14281	M	A	C	LS
	Equus burchellii granti	247	RBINS	33386	U	A	U	LS
	Equus grevyi	400	RBINS	32166	M	A	C	LS
	Equus quagga boehmi	247	RBINS	12129	M	A	W	LS
	Equus quagga chapmani	247	RBINS	1218	F	A	C	LS
	Equus quagga quagga	247	IMNH	R2425	U	A	U	LS*
	Equus zebra hartmannae	310	RBINS	3974	M	S	C	LS

Note:
Abbreviations: Sex–F, female; M, male; U, unknown. Age–A, adult; S, sub-adult. Condition–W, wild; C, captive; U, unknown. 3D acquisition–LS, laser scanner; SL, structured light surface scanner; P, photogrammetry; CT, CTscan. Stars indicate specimens retrieved on MorphoSource deposit. Institutional codes–AMNH, American Museum of Natural History. BICPC, Powell Cotton Museum, Birchington-on-Sea. IMNH, Idaho Museum of Natural History, Pocatello. MNHN, Muséum National d'Histoire Naturelle, Paris. MVZ, Museum of Vertebrate Zoology, Berkeley. NHMUK, Natural History Museum, London. NMB, Naturhistorisches Museum Basel, Basel. RBINS, Royal Belgian Institute of Natural Sciences, Brussels.

d'Histoire Naturelle, Paris (UMS 2700; GE phoenix|X-ray v|tome|xs 240), with reconstructions performed using the CT-agent software (Nikon Metrology, Leuven, Belgium), and DATOX/RES software (phoenix datos|x). Bone surfaces were extracted as meshes using Avizo 9.4 (*https://www.thermofisher.com/fr/fr/home/electron-microscopy/products/software-em-3d-vis/avizo-software.html*; Thermo Fisher Scientific, Waltham, MA, USA). Three specimens were retrieved on the online deposit MorphoSource (see Table 1 for details). Only right bones were selected for digitization; when unavailable, we selected left bones instead and mirrored the 3D models before analysis using MeshLab (v2022.02; *Cignoni et al., 2008*). ARK identifiers of each 3D model are provided in Table ST1.

3D geometric morphometrics

We analysed the shape variation of our sample using a 3D geometric morphometrics approach. This widely used methodology allows to quantify and visualize the morphological differences between objects by comparing the spatial coordinates of landmarks placed on them (*Adams, Rohlf & Slice, 2004*; *Zelditch et al., 2012*; *Mitteroecker & Schaefer, 2022*). The shape of the patella was quantified by placing a set of anatomical landmarks and curve and surface sliding semi-landmarks on the meshes, as described by *Gunz, Mitteroecker & Bookstein (2005)* and *Botton-Divet et al. (2016)*. Anatomical landmarks and curves were placed on meshes using the IDAV Landmark software (v3.0–*Wiley et al., 2005*). We defined six anatomical landmarks associated with two curves allowing to cover the shape diversity of the patella in modern perissodactyls (Fig. 3). We
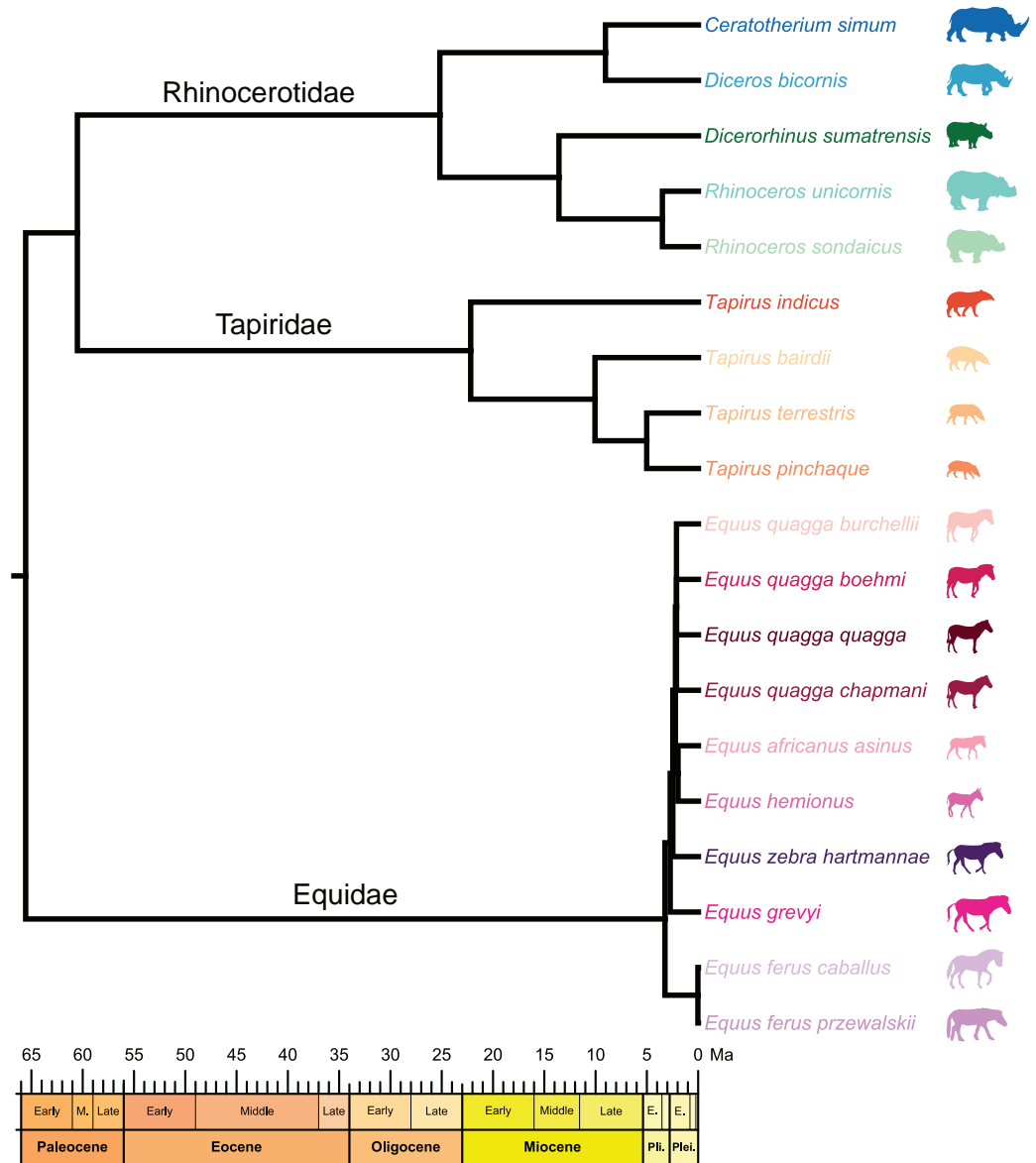
Figure 2 Composite cladogram of the sampled species. Branch lengths and relations based on *Steiner & Ryder (2011)*, *MacLaren et al. (2018)*, *Bai et al. (2020)*, *Cirilli et al. (2021)*, *Antoine et al. (2021)*, *Liu et al. (2021)*, *Pandolfi et al. (2021)*. Silhouettes of *C. simum, Dc. bicornis, Ds. sumatrensis, E. z. hartmannae, E. grevyi, R. sondaicus, R. unicornis* and *T. indicus* are personal creations. All other silhouettes provided by *www.phylopic.org* under the Creative Commons license. Full-size 🖼 DOI: 10.7717/peerj.18067/fig-2

evaluated the relevance of these anatomical landmarks to describe the shape by conducting repeatability tests. We considered three specimens of *Ds. sumatrensis* chosen to display the closest morphology. We successively digitized ten times the anatomical landmarks on the three specimens to obtain thirty replications of the landmark datasets. We superimposed these landmark configurations using a generalized Procrustes analysis (GPA, see below) then performed a principal component analysis (PCA) to visualise the placement of each repeated set of measurement relatively to each other. It appeared clearly that the variation
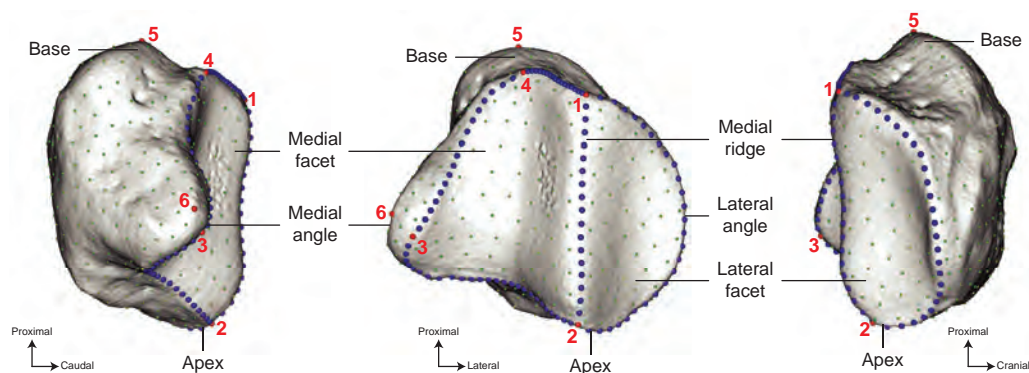
Figure 3 Location of the landmarks used for the analyses. A total of six anatomical landmarks (red spheres), 103 curve sliding (blue spheres) and 461 surface sliding (green spheres) semi-landmarks were placed on the patella. Designation of the anatomical landmarks–1, Most proximal point of the medial ridge; 2, most distal point of the medial ridge; 3, most medial point of the medial articular surface; 4, most proximal point of the medial articular surface; 5, most proximal point of the base; 6, most medial point of the medial angle.
Full-size ☑ DOI: 10.7717/peerj.18067/fig-3

within specimens was lower than between specimens, confirming the relevance of our landmarks to precisely describe the shape variation (see Fig. S1).

Anatomical landmarks and curve sliding semi-landmarks were placed on each specimen. A template was created for the placement of the surface sliding semi-landmark on each patella. A specimen (*C. simum* AMNH M-51854) was selected as the initial specimen on which all anatomical landmarks, curve and surface sliding semi-landmarks were placed. This specimen was selected for its average shape and size allowing to ensure the correct placement of the landmarks on all the other specimens despite the great variation of size and shape in the sample. It was then used as a template for the projection of surface sliding semi-landmarks on the surface of all other specimens. Projection was followed by a relaxation step ensuring that projected points matched the surface of the meshes. Curve and surface semi-landmarks were then slid by minimizing the bending energy of a thin plate spline (TPS) between each specimen and the template at first, then four times between the result of the previous step and the Procrustes consensus of the complete dataset (see *Gunz, Mitteroecker & Bookstein, 2005*; *Botton-Divet et al., 2016* for details regarding this process). Once this process was complete, all landmarks could be treated as geometrically homologous. We then performed a GPA to remove the effect of relative size, location and orientation of the different landmark conformations (*Gower, 1975*; *Rohlf & Slice, 1990*). Projection, relaxation, sliding processes and GPA were conducted using the "Morpho" package (v2.10; *Schlager, 2017*) in the R environment (v4.2.1; *R Core Team, 2014*). Details of the function parameters used are provided in the R code available as Supplemental Data.

Superimposed conformations of landmarks were used to compute a PCA in order to reduce dimensionality (*Gunz & Mitteroecker, 2013*) (function "procSym" in the "Morpho" package). PC scores where then used to compute neighbour-joining (NJ) trees and morphospaces allowing to visualise the distribution of each individual relatively to each other. To visualise how shape varies in association with the specimen distribution, we

computed theoretical shapes associated with both minimal and maximal values for the two first PCs using a TPS deformation of a template mesh. To emphasize the location of the main shape changes on the patella among the sample, we displayed the vectors of displacement between all landmarks of the two theoretical shapes using the "rgl" package (v0.109.6; *Adler & Murdoch, 2020*). As described by *Botton-Divet (2017)* and *Pintore et al. (2021)*, we applied a gradient of colour to these segments according to their distance to highlight which parts varied the most, these segments being displayed directly onto the superimposed theoretical shapes (see the R code available as Supplemental Data for details of the process). Detailed NJ trees and PCA plots for equids and tapirs only are provided as Supplemental Data.

We explored the relation between shape and specific attribution, sex, size, type of gallop and presence/absence of a knee-locking mechanism (see below). Permutational analyses of variance (PERMANOVAs) (*Costa-Pereira et al., 2016*; *Anderson, 2017*) were performed on PC scores against the specific attribution and sex class to test for the impact of these parameters on the patellar shape. We also performed a PERMANOVA on PC scores against the type of gallop (transverse and rotary) to address the effect of locomotor mode. As the presence of a knee-locking mechanism is distributed exactly as the type of gallop (*i.e.*, tapirs have a rotary gallop and no knee-locking mechanism, while equids and rhinos have a transverse gallop and a knee-locking mechanism), we did not test for this last parameter, as the result would have been redundant with the one previously described. We used the function "adonis2" in the "vegan" package (v.2.6-4) to perform PERMANOVAs (using the Euclidian method and removing lacking sex attribution with the argument "na.exclude") (*Dixon, 2003*). We explored allometric variation (*i.e.*, shape variation linked to size; *Hallgrímsson et al., 2009*; *Zelditch et al., 2012*; *Mitteroecker et al., 2013*; *Klingenberg, 2016*) within our sample using different approaches. Pearson's correlation tests were performed to test for correlation between the scores of the two first PCs and the centroid size of the specimens. We performed a Procrustes ANOVA (a linear regression model using Procrustes distances between species instead of covariance matrices; *Goodall, 1991*; *Adams & Otárola-Castillo, 2013*) with 1,000 permutations and a sequential sum of squares to quantify the shape variation related to the centroid size to highlight the influence of centroid size on the global shape variation. Procrustes ANOVA has been performed using the function "procD.lm" in the "geomorph" package. This set of analyses (PERMANOVA, Pearson's correlation tests, Procrustes ANOVAs) was applied respectively on rhinoceroses alone and on all perissodactyls.

Proxies of body mass

In the absence of most of the mass values of the specimens constituting our sample, we chose two proxies of body mass: (1) the centroid size (CS) of each patella, generally used to address allometric variation, defined as the square root of the sum of the square of the distance of each point to the centroid of the landmark set (*Zelditch et al., 2012*); it is generally considered as a good proxy of the body mass of the animal; and (2) the minimal

femoral circumference (FC) of each specimen, a measurement classically used in equations of body mass estimation. Indeed, the femur being a crucial bone for weight support in quadrupeds, its circumference is known to strongly covary with body mass (*Anderson, Hall-Martin & Russell, 1985*; *Scott, 1990*; *Damuth & MacFadden, 1990*; *Campione & Evans, 2012*; *Campione, 2017*). FC therefore provides a proxy of mass relatively independent of the patella itself. We used a Pearson's correlation test to evaluate the correlation between CS and FC. We also performed Procrustes ANOVAs as described above using FC instead of CS to quantify their respective relations with shape variation, both on rhinos alone and on all perissodactyls.

Phylogenetic framework

To test the presence of a phylogenetic signal in our shape data, we constructed a composite cladogram using trees previously computed on molecular data and craniodental and postcranial characters (Fig. 2). Branch relations, lengths and occurrence dates were retrieved and merged following phylogenetic reconstructions proposed in recent works (*Steiner & Ryder, 2011*; *MacLaren et al., 2018*; *Bai et al., 2020*; *Cirilli et al., 2021*; *Antoine et al., 2021*; *Liu et al., 2021*; *Pandolfi et al., 2021*). The phylogenetic relation of *Ds. sumatrensis* relatively to the other modern species has long been debated (see *Mallet et al., 2019*). As recent works based on molecular and morphological data agreed on the phylogenetic position of this species (*Antoine et al., 2021*; *Liu et al., 2021*; *Pandolfi et al., 2021*), we considered here *Ds. sumatrensis* as sister taxon of the *Rhinoceros* genus.

We addressed the effect of phylogenetic signal on shape and centroid size in our dataset. Given the small numbers of rhino species (five), tests for phylogenetic signal were only performed on all perissodactyl species. For species represented by several specimens, we computed species mean shapes (*Botton-Divet et al., 2017*; *Serio, Raia & Meloro, 2020*; *Mallet et al., 2021*, *2022*). We computed a first GPA with all specimens of the second subsample (all perissodactyls) as described previously, then we computed the Procrustes consensus (or mean shape) of each species in this geometric space. These Procrustes consensuses were superimposed in a second GPA before computing a new PCA. We then addressed the effect of phylogeny on mean centroid sizes per species with the univariate K statistic (*Blomberg et al., 2003*), using the function "phylosig" in the "phytools" package (*Revell, 2012*). We also addressed the effect of phylogenetic relationships on shape data using the multivariate K statistic (K_{mult}) on PC scores (*Adams, 2014*). K_{mult} index allows the comparison between the rate of observed morphological change and that expected under a Brownian motion on a given phylogeny (*Blomberg et al., 2003*; *Adams, 2014*). K_{mult} was computed using the function "physignal" in the "geomorph" package (v4.0.4–*Adams & Otárola-Castillo, 2013*).

According to recent works calling for a continuous approach of the *p* value (*Wasserstein, Schirm & Lazar, 2019*; *Ho et al., 2019*), statistic tests were considered as significant for *p* values ≤ 0.05 but we chose to mention and comment results having a *p* value between 0.05 and 0.10 as well.

RESULTS

Shape variation within rhinoceroses

The distribution of the specimens both in the NJ tree and in the morphospace shows a clear distinction between African and Asiatic rhinos. Along the NJ tree (Fig. 4), specimens of *C. simum* and *Dc. bicornis* plot together and oppose to *Ds. sumatrensis*, *R. sondaicus* and *R. unicornis*. The *Dc. bicornis* and *C. simum* specimens are mixed, as are the *R. sondaicus* and *R. unicornis* specimens. Those of *Ds. sumatrensis* form an isolated and more homogeneous cluster. The morphospace of the first two axes of the PCA, representing 47.5%, displays a similar structure (Fig. 5A). PC1, which carries 33.6% of the global variance, separates African rhinos towards negative values from Asiatic rhinos towards positive values. *C. simum*, occupies the highest negative values of the axis while *R. unicornis* and *R. sondaicus* occupy the highest positive values. *Ds. sumatrensis* specimens partially overlap *R. unicornis* along the PC1. PC2 represents 13.9% of the variance and is structured by the isolation of *Ds. sumatrensis* towards the highest positive values, while all other species overlap around lower values.

A Pearson's correlation test indicates that PC1 ($r = -0.41$; $p = 0.03$) and PC2 ($r = -0.55$; $p < 0.01$) are correlated with the centroid size (Table 2). The PERMANOVA of PC scores against the specific attribution and sex of the specimen confirms a highly significant correlation between the shape of the patella and the specific attribution ($R^2 = 0.59$; $p < 0.01$), but no correlation with the sex attribution ($p = 0.47$) (Table 3).

Shape variation along PC1 is mainly related to the proximodistal extension of the base and the aspect of the medial angle (Fig. 5B-a). Towards minimal values, patella display a rounded and smooth general aspect. The articular surface for the femur is concave and has a convex cranial surface. The proximal end of the medial articular surface slightly exceeds that of the lateral articular surface. The medial ridge is sigmoid in medial view, with a rounded distal part. The base is mediolaterally broad and extends slightly proximally, being only little higher than the proximal border of the articular surface. The medial angle is rounded and smooth, pointing mediodistally. Towards maximal values, the patella has a more angular general aspect. The cranial surface of the patella forms a straight dorsoventral line, before displaying a caudoventral inflexion towards the apex. The proximal end of the medial articular surface exceeds greatly that of the lateral articular surface. The medial ridge is straight in medial view, forming an almost flat relief caudally to the apex. The base forms a saliant triangle with a narrow base, and a right angle markedly higher than the proximal border of the articular surface. The medial angle forms a rounded protrusion pointing strictly medially.

Shape variation along PC2 is mainly dominated by changes in the antero-posterior broadness of the patella, the proximodistal extension of the base and the apex, and the aspect of the medial angle (Fig. 5B-b). Towards minimal values, the patella has a robust general aspect, especially antero-posteriorly, with a base extending strongly proximally. The articular surface for the femur has a medial part pointing in proximal direction. In medial view, the anterior surface of the patella follows a straight line from the base before forming a marked obtuse angle towards the apex. The proximal end of the medial articular
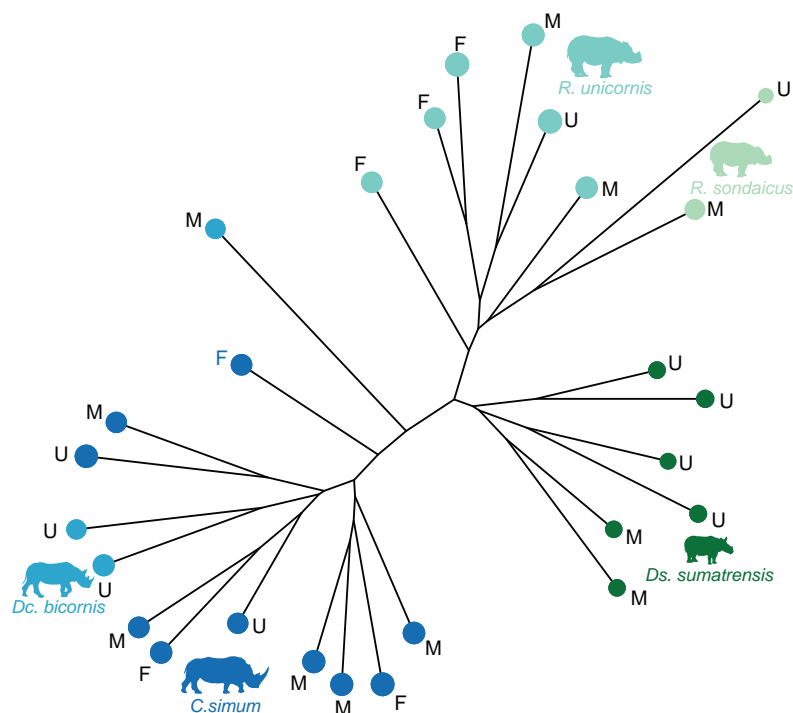
Figure 4 Neighbour-joining tree computed on all PC scores obtained from the PCA performed on shape data of rhinoceroses. Colour code follows Fig. 2. Letters indicate sex attribution as in Table 1 (F, female; M, male; U, unknown). Point size is proportional to the log centroid size of each specimen. Silhouettes of *C. simum, Dc. bicornis, Ds. sumatrensis, E. z. hartmannae, E. grevyi, R. sondaicus, R. unicornis* and *T. indicus* are personal creations. All other silhouettes provided by *www.phylopic.org* under the Creative Commons license. Tree generated by our R code provided as Supplemental Data.

Full-size 🖼 DOI: 10.7717/peerj.18067/fig-4

surface exceeds markedly that of the lateral articular surface. The medial ridge is slightly concave, almost straight, in medial view. The base is thick, broadly triangular and forms a saliant proximal protrusion. The medial angle forms a broad triangle pointing directly medially. The apex is thick and short. Towards maximal values, the patella is flatter antero-posteriorly, with a prominent protrusion of the apex. The articular surface for the femur has an irregular triangular shape pointing distally. The anterior surface of the patella forms a convex surface from the base to the apex. The proximal end of the medial articular surface slightly exceeds that of the lateral articular surface. The medial ridge is concave in medial view and forms a convex relief above the apex. The base is very short and slightly extended proximally. The medial angle forms a large, rounded protrusion pointing medially. The apex expands largely and forms a saliant relief directed posterodistally.

The regression plot of the Procrustes ANOVA performed on shape against log centroid size shows a marked difference between Asiatic and African rhinos (Fig. 6A). Towards maximal CS values, *C. simum* and *Dc. bicornis* plot above the line while most *R. unicornis* plot below the line. Towards minimal CS values, most *Ds. sumatrensis* plot below the line or close to it, except for one individual showing a lower centroid size compared to other specimens. Positions of *R. sondaicus* relatively to the line are hard to interpret, given the small number of individuals and the isolation of an unusually small specimen towards
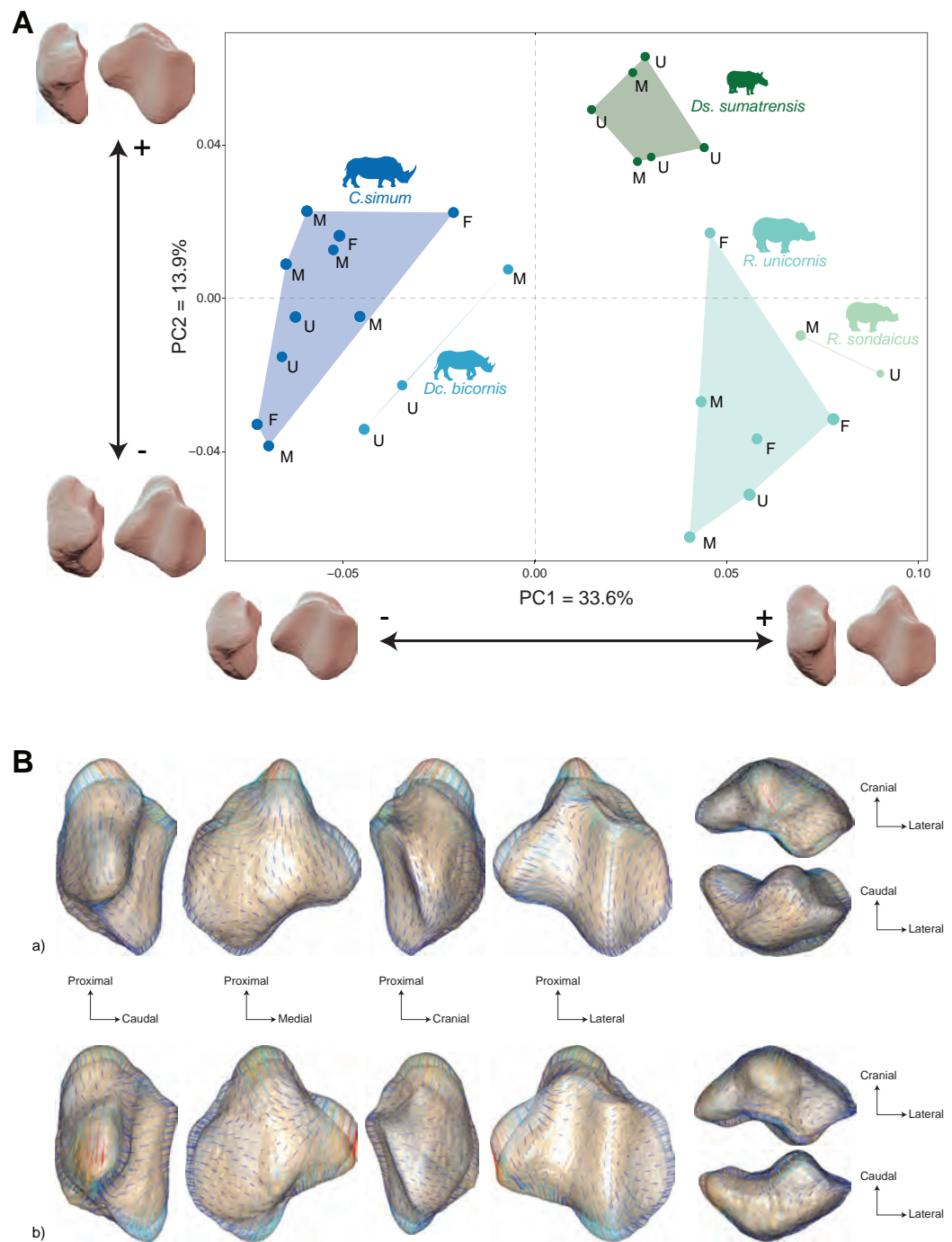
Figure 5 Results of the PCA performed on morphometric data of rhinoceroses and associated shape variation. (A) Morphospace of the two first axes of the PCA with minimal and maximal theoretical shape associated with this variation (respectively in medial and caudal views). Colour codes follow Fig. 2. Letters indicate sex attribution as in Table 1. Point size is proportional to the log centroid size of each specimen. Silhouettes of *C. simum, Dc. bicornis, Ds. sumatrensis, E. z. hartmannae, E. grevyi, R. sondaicus, R. unicornis* and *T. indicus* are personal creations. All other silhouettes provided by *www.phylopic.org* under the Creative Commons license. (B) Morphological variation between minimal (light brown) and maximal (light grey) theoretical shapes along a) PC1 and b) PC2 respectively in medial, cranial, lateral, caudal, dorsal (top) and ventral (bottom) views. Intensities of landmark displacements are shown with vector colorations ranging from blue (low distance) to red (high distance). Plot and theoretical 3D

Table 2 Results of the Pearson's correlation tests between the log-transformed centroid size and the two first principal components of the PCA, for rhinoceroses only and all perissodactyls respectively.

	Component	r	t	dF	P
Rhinoceroses	PC1	−0.41	−2.24	25	0.03
	PC2	−0.55	−3.278	25	<0.01
All perissodactyls	PC1	−0.61	−5.60	52	<0.01
	PC2	−0.48	−3.96	52	<0.01

Note:
Abbreviations: r, Pearson's correlation coefficient value; t, Student distribution value; dF, degrees of freedom; P, *p* value. Significant results are indicated in bold.

Table 3 Results of the PERMANOVAs performed on PC scores against specific attribution and sex, for rhinoceroses only and all perissodactyls respectively, and on PC scores against type of gallop for all perissodactyls.

		Df	Sum of squares	R²	F	P
Rhinoceroses	Species	**4**	**0.08**	**0.59**	**4.20**	**<0.01**
	Sex	1	<0.01	0.03	0.90	0.47
	Residuals	11	0.05	0.38		
	Total	16	0.13	1		
All perissodactyls–Sex	Species	**15**	**0.62**	**0.86**	**8.34**	**<0.01**
	Sex	1	<0.01	<0.01	0.74	0.563
	Residuals	20	0.10	0.14		
	Total	36	0.72	1		
All perissodactyls–Type of gallop	Gallop	**1**	**0.43**	**0.40**	**35.36**	**<0.01**
	Residuals	52	0.63	0.60		
	Total	53	1.05	1		

Note:
Abbreviations: dF, degrees of freedom; R², coefficient of partial determination; F, F-statistics; P, *p* value. Significant results are indicated in bold.

minimal CS values. Shape variation associated with centroid size mainly involves changes in the general proportions of the patella, as well as the relative development of the base, the medial angle and, at a lesser extent, the apex (Figs. 6A and 6B). Towards high values of centroid size, the patella broadens antero-posteriorly, showing a more rounded and smooth general aspect. The base is broad and thick, slightly developed proximally, forming a convex relief posteriorly to the articular surface. The medial angle forms a smooth triangle pointing medially, distally, and posteriorly. The apex appears short and broad.

Moreover, the shape is significantly correlated with centroid size ($p < 0.01$) but centroid size accounts for only 12% of the global shape variance ($R^2 = 0.12$) (Table 4) The regression plot highlights a signal strongly driven by *Ds. sumatrensis* and one specimen of *R. unicornis*. When removing these two species from the Procrustes ANOVA, the correlation
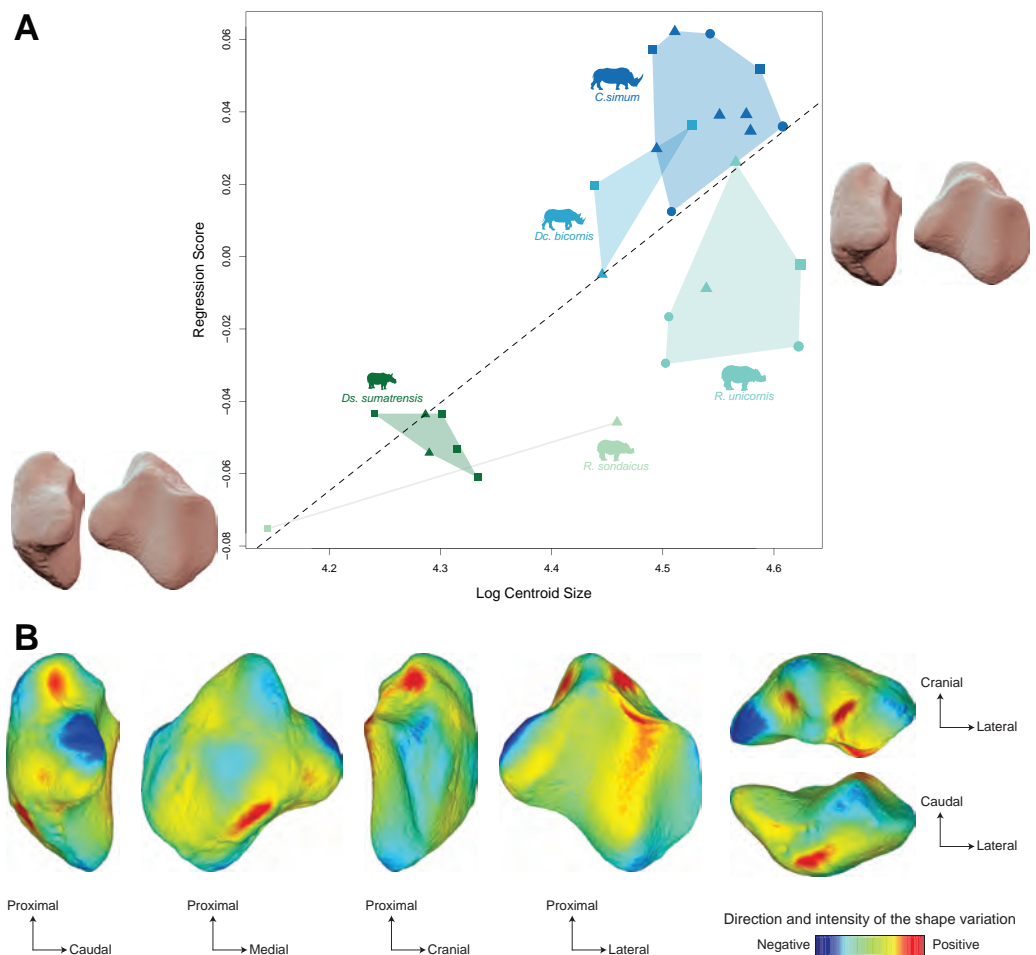
Figure 6 **Results of the Procrustes ANOVA on shape data against log-transformed centroid size (CS) for rhinos.** (A) Regression plot with theoretical shapes associated with minimum and maximum fitted values (respectively in medial and caudal views). Colour code follows Fig. 2. Point size is proportional to the log centroid size of each specimen. Symbols indicate the sex attribution (triangle: male; circle: female; square: unknown). Silhouettes of *C. simum, Dc. bicornis, Ds. sumatrensis, E. z. hartmannae, E. grevyi, R. sondaicus, R. unicornis* and *T. indicus* are personal creations. All other silhouettes provided by *www. phylopic.org* under the Creative Commons license. (B) Colour maps of the location and intensity of the shape deformation. The shape associated with the maximal CS value of the Procrustes ANOVA was coloured depending on its distance to the shape associated with the minimal value. Green indicates no deformation; blue indicates a negative deformation of high intensity; red indicates a positive deformation of high intensity. Plot and theoretical 3D models generated by our R code provided as Supplemental Data. Plot and theoretical 3D models generated by our R code provided as Supplemental Data (using the specimen *Dicerorhinus sumatrensis* AMNH M-81892 as a template for deformation of the meshes).
Full-size 🖼 DOI: 10.7717/peerj.18067/fig-6

between shape data and size is not significant anymore ($p = 0.18$). However, the small number of individuals for these species prevents us to go further on this question. In accordance with the strong correlation between centroid size and femoral circumference (Pearson's correlation test; $r = 0.75$, $p < 0.01$), very similar results are obtained when considering the log of the minimal femoral circumference instead of the centroid size in the Procrustes ANOVA (Table 4). The regression plot of shape data against FC led to an almost similar distribution of the specimens than that obtained with CS, African rhinos

Table 4 Results of the Procrustes ANOVAs on shape data against log centroid size and femoral circumference respectively, for rhinoceroses only and all perissodactyls respectively.

		dF	Sum of squares	R²	F	Z	P
Rhinoceroses only	Log centroid size	1	**0.03**	**0.12**	3.37	2.57	<0.001
	Residuals	25	0.19	0.88			
	Total	26	0.22				
	Log femoral circumference	**1**	**0.02**	**0.12**	3.20	2.33	0.01
	Residuals	24	0.18	0.88			
	Total	25	0.21				
All perissodactyls	Log centroid size	1	**0.23**	**0.22**	14.74	4.13	<0.01
	Residuals	52	0.81	0.78			
	Total	53	1.04				
	Log femoral circumference	1	**0.25**	**0.26**	17.27	4.40	<0.01
	Residuals	50	0.73	0.74			
	Total	51	0.99				

Note:
Abbreviations: dF, degrees of freedom; R², coefficient of determination; F, F-statistics; Z, Z score; P, *p* value. Significant results are indicated in bold.

plotting above the regression line while the two *Rhinoceros* species plot below and *Ds. sumatrensis* isolates towards minimal FC values (see Fig. S2A). Shape variation associated with FC are very similar to that observed with CS too, with an even more marked modification of the medial ridge of the patella (see Fig. S2B).

Shape variation between all perissodactyls

When considering all perissodactyls, shape data carries a significant but low phylogenetic signal ($K_{mult} = 0.141$, $p < 0.01$), while the mean centroid size per species does not carry a significant phylogenetic signal ($p = 0.57$). The distribution of the specimens both in the NJ tree and in the morphospace strictly separates rhinos, equids, and tapirs (Fig. 7). Among rhinos, the repartition previously observed is conserved, with clustering African and Asiatic rhinos, and one *Dc. bicornis* clustering close to *C. simum*. The species clustering is far less clear among tapirs, although the low number of specimens limits the scope of our observations. All specimens of *Tapirus indicus*, the largest and only Asiatic species of tapir, cluster together, while the other three species are less clustered. When considered separately, the different tapir species discriminate well on the PCA but stay unclustered on the NJ tree (see Fig. S3). Among equids, most *E. quagga* plot together, as do most donkeys (*E. africanus asinus*, *E. hemionus*), far from *E. quagga*. Between them, *E. grevyi* plot together with horses (*E. ferus caballus* and *E. ferus przewalskii*). Two larger specimens of *E. asinus* are mixed among horses and quaggas, respectively. When considered alone, equids show a strong mixing, despite most zebras and horses grouping together, respectively (see Fig. S4).

The morphospace of the first two axes of the PCA, representing 65.8% of the global variance, is structured by a strict separation between the three perissodactyl families, with overlap between the species within each family (Fig. 8A). PC1 carries 42.7% of the global
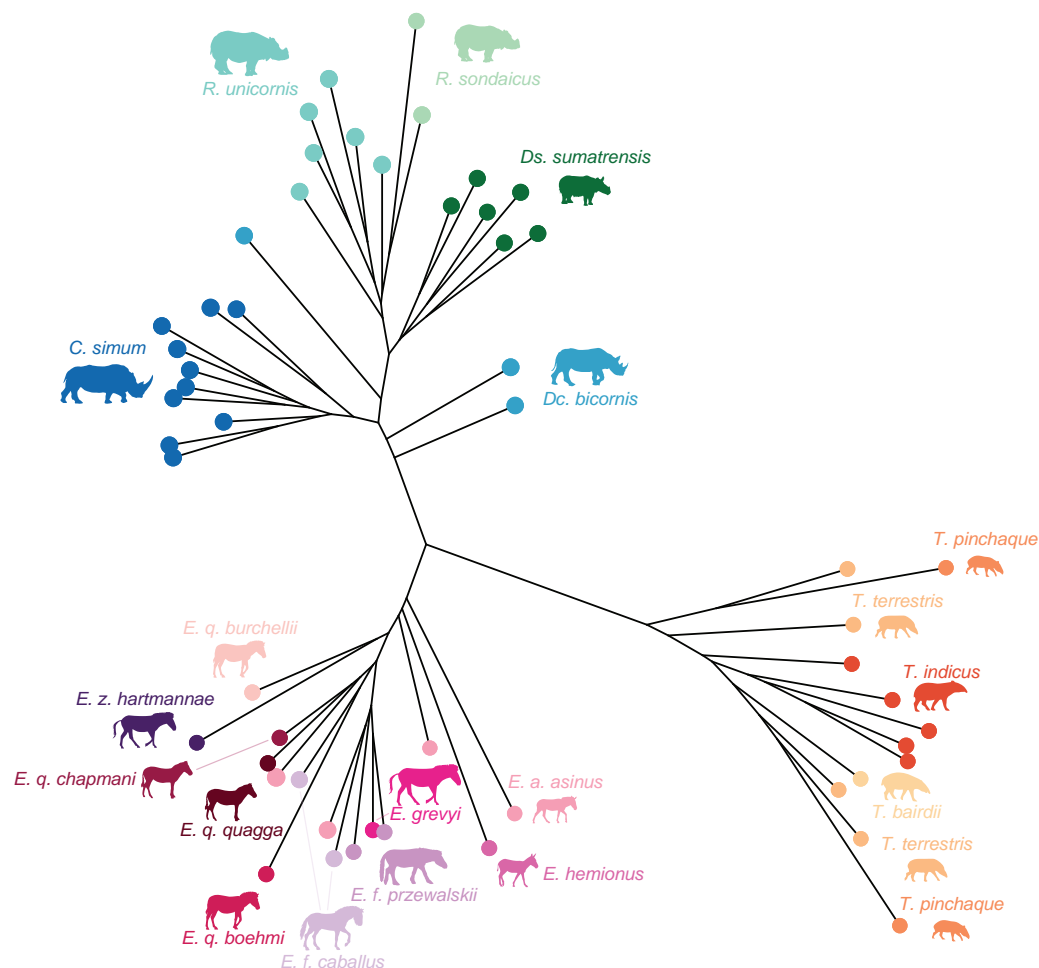
Figure 7 Neighbour Joining tree computed on all PC scores obtained from the PCA performed on shape data of all perissodactyls. Colour code follows Fig. 2. Symbols indicate age class as in Table 1 (triangle: subadult; circle: adult). Point size is proportional to the log centroid size of each specimen. Silhouettes of *C. simum, Dc. bicornis, Ds. sumatrensis, E. z. hartmannae, E. grevyi, R. sondaicus, R. unicornis* and *T. indicus* are personal creations. All other silhouettes provided by *www.phylopic.org* under the Creative Commons license. Tree generated by our R code provided as Supplemental Data.

Full-size 🖼 DOI: 10.7717/peerj.18067/fig-7

variance and separates rhinos and equids in the negative part of the axis from tapirs which are positioned in the positive part. All equids group together with no clear structure, except for *E. hemionus*, plotting outside the equid cluster (an observation confirmed on the PCA plot of equids alone; see Fig. S4). Among each family, the separation between species is far less clear. Rhinos, to the exclusion of *Ds. sumatrensis* and *C. simum*, although to a lesser extent, have PC1 scores that overlap those of Equidae. Among tapirs, *T. pinchaque* isolates slightly from other species, which can also be observed on the PCA plot of tapirs alone (Fig. S3). Along PC2, which accounts for 23% of the variance, rhinos, and tapirs in the negative part of the axis are separated from equids in the positive part.

PC1 and PC2 are both highly correlated with the centroid size (Pearson's correlation test: r = −0.61; p < 0.01 and r = −0.48; p < 0.01, respectively) (Table 2). PERMANOVA
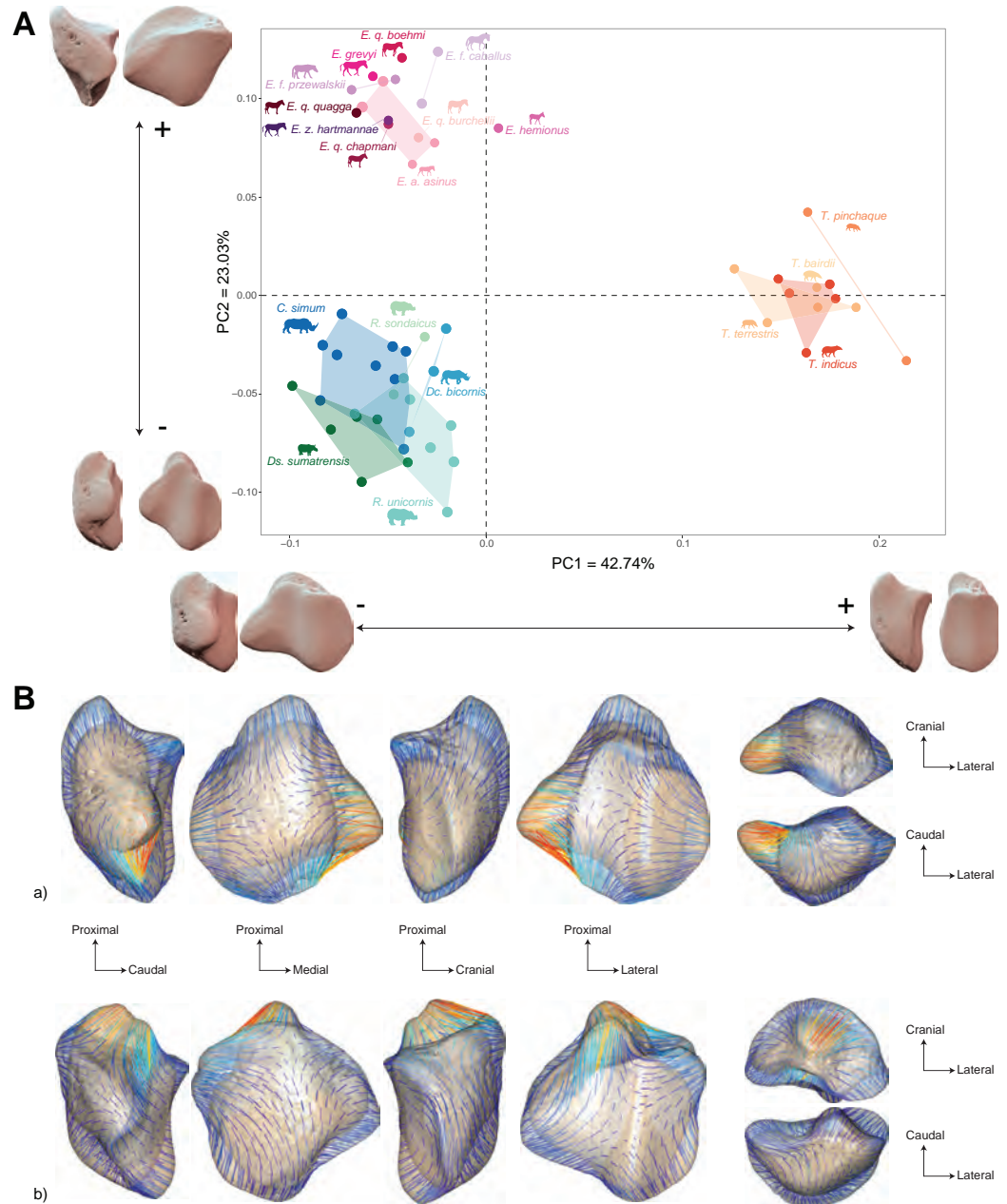
Figure 8 Results of the PCA performed on morphometric data of all perissodactyls and associated shape variation. (A) Morphospace of the two first axes of the PCA with minimal and maximal theoretical shape associated with this variation (respectively in medial and caudal views). Colour codes follow Fig. 2. Point size is proportional to the log centroid size of each specimen. Silhouettes of *C. simum, Dc. bicornis, Ds. sumatrensis, E. z. hartmannae, E. grevyi, R. sondaicus, R. unicornis* and *T. indicus* are personal creations. All other silhouettes provided by *www.phylopic.org* under the Creative Commons license. (B) Morphological variation between minimal (light brown) and maximal (light grey) theoretical shapes along a) PC1 and b) PC2 respectively in medial, cranial, lateral, caudal, dorsal (top) and ventral (bottom) views. Intensities of landmark displacements are shown with vector colorations ranging from blue (low distance) to red (high distance). Plot and theoretical 3D models generated by our R code provided as Supplemental Data (using the specimen *Diceros bicornis* NHMUK ZD 1879.9.26.6 as a template for deformation of the meshes). Full-size 🖼 DOI: 10.7717/peerj.18067/fig-8

confirms an extremely high and significant correlation between the shape of the patella and the specific attribution ($R^2 = 0.86$; $p < 0.01$), as well as a significant although lower correlation between shape and type of gallop ($R^2 = 0.40$; $p < 0.01$). Conversely, sex attribution is not significantly correlated with shape data ($p = 0.56$) (Table 3).

Shape variation along PC1 is mainly related to the degree of asymmetry of the patella, the extension of the medial angle, and the anteroposterior broadening of the base (Fig. 8B-a). Both extreme shapes reflect respectively rhino and tapir morphotypes. Towards negative values, the anterior surface is relatively flat, with a straight anterior border forming a well-marked angle (around 125°) towards the apex. The articular surface for the femur is globally rounded and smooth. The medial ridge is sigmoid and slightly concave in medial view. The base is broad mediolaterally and extends slightly proximally. The medial angle is rounded and smooth and extends strongly mediodistally. The apex is broad and massive antero-posteriorly, and slightly expands distally. Towards positive values, the theoretical shape of the patella is strongly symmetric, with no medial angle. The anterior surface is strongly and curved from the base to the apex. The articular surface for the femur is globally rectangular with symmetric medial and lateral facets. The medial ridge is concave in medial view, the rounded distal part towards the apex protruding only slightly. The base is well-developed and broad antero-posteriorly, ending in a marked knob pointing medio-proximally. The medial angle is almost absent, reduced to a smooth relief along the medial border of the articular surface. The apex is thin, wedge-shaped, slightly extended distally relatively to the articular surface.

Along PC2, shape variation is mainly related to the development and aspect of the base and of the medial angle (Fig. 8B-b). Towards minimal values, the shape displays a "rhino-like" general aspect with a marked mediolateral compression. The base forms a salient relief extending markedly proximally. The medial angle is rounded, smooth and extends in medial direction. Towards maximal values, patellae are shaped like a triangular-based pyramid. The anterior surface is strongly convex, extending markedly anteriorly. In medial view, the anterior border of the patella forms a 45-degrees downward slope towards the apex. The articular surface for the femur forms a marked angle pointing medially. The proximal end of the medial articular surface is situated below that of the lateral articular surface. The medial ridge forms a smooth sigmoid in medial view, the proximal part overhanging the articular surface in posterior direction. The base expands massively in anterior direction and forms a large flat surface strongly inclined distally towards the medial angle. No marked relief is visible on the surface of the base. The medial angle is broad and rounded, extending strongly medio-distally. The apex is short antero-posteriorly. Views of patellar mean shapes for each species of the dataset are displayed in the Fig. S5.

Shape is significantly correlated with centroid size (Procrustes ANOVA: $R^2 = 0.22$; $p < 0.01$) (Table 4). The regression plot of shape against log centroid size shows a limited spreading of the specimens around the regression line (Fig. 9A). Towards maximal CS values, *C. simum* and *Ds. sumatrensis* are now mostly above the regression line while *R. unicornis* plot mostly below. Once again, the position of the few specimens of *Dc. bicornis* and *R. sondaicus* remains hard to interpret. Almost all equids plot above the regression line
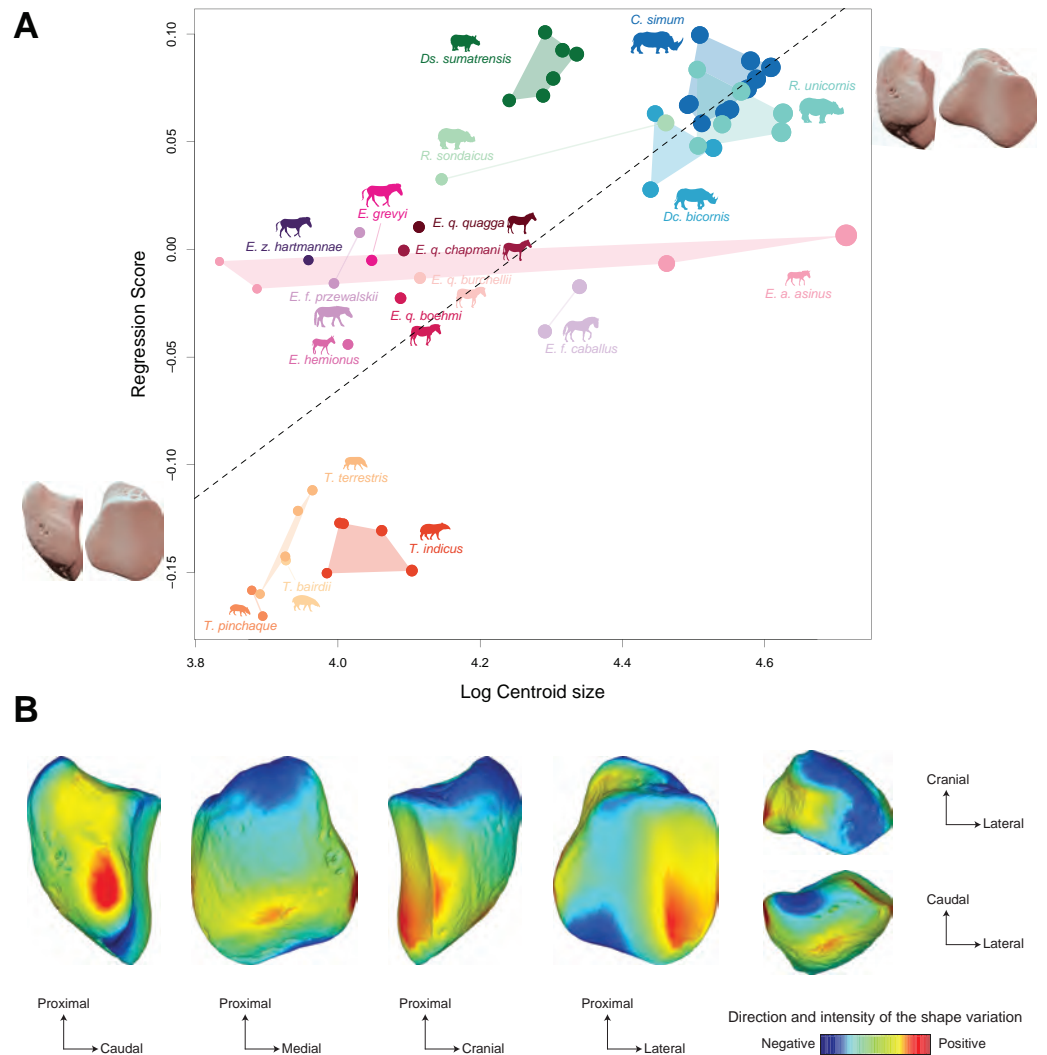
Figure 9 Results of the Procrustes ANOVA on shape data against log-transformed centroid size (CS) for all perissodactyls. (A) Regression plot with theoretical shapes associated with minimum and maximum fitted values (respectively in medial and caudal views). Colour code follows Fig. 2. Point size is proportional to the log centroid size of each specimen. Silhouettes of *C. simum, Dc. bicornis, Ds. sumatrensis, E. z. hartmannae, E. grevyi, R. sondaicus, R. unicornis* and *T. indicus* are personal creations. All other silhouettes provided by *www.phylopic.org* under the Creative Commons license. (B) Colour maps of the location and intensity of the shape deformation. The shape associated with the minimal CS value of the Procrustes ANOVA was coloured depending on its distance to the shape associated with the maximal value. Green indicates no deformation; blue indicates a negative deformation of high intensity; red indicates a positive deformation of high intensity. Plot and theoretical 3D models generated by our R code provided as Supplemental Data (using the specimen *Diceros bicornis* NHMUK ZD 1879.9.26.6 as a template for deformation of the meshes).   Full-size ⬛ DOI: 10.7717/peerj.18067/fig-9

with few exceptions: *E. caballus* and two *E. asinus*, one of which being a draught breed with the highest CS value of the sample. All tapirs plot together below the regression line and are ordered from the least body mass to the greatest one along the centroid size values. Shape variation associated with centroid size mainly reflects differences between tapirs for minimal values and rhinos for maximal values. Changes in centroid size among

perissodactyls involve changes in the general asymmetry of the patella, the relative development of the medial angle and the cranio-caudal broadening of the bone (Figs. 9A and 9B). As for rhinos alone, the femoral circumference among all perissodactyls is highly correlated to the centroid size of the patella (r = 0.88, $p < 0.01$). Consequently, shape is also correlated with femoral circumference (Procrustes ANOVA: R^2 = 0.26; $p < 0.01$) (Table 4), with a regression plot and associated shape variation very similar to those observed for CS (see Fig. S6).

DISCUSSION

Intra- and interfamily variation of shape

Our results highlight a marked distinction between African and Asiatic rhino clades, despite important weight variations within these two groups, suggesting that the shape of the patella among rhinoceroses is highly related to phylogenetic affinities prior to body mass. Each rhino species possesses a unique patellar shape. This supports our first hypothesis that interspecific variation of patellar shape is stronger than intraspecific variation of patellar shape. In the hindlimb, the patella articulates directly with the trochlear groove of the femur, while it is linked with the tibia by only ligaments. Moreover, the patella in mammals is known to separate from the femur in the early developmental stages of the embryo (Eyal et al., 2015, 2019). The patella and the femur are therefore strongly bonded bones, both on functional and developmental aspects. These observations are congruent with previous results suggesting that femoral shape variation is also more greatly driven by phylogenetic affinities over body mass, especially the distal part directly linked with the patella (Mallet et al., 2019, 2022). This observation is however less clear for Ds. sumatrensis, as this rhino is the lightest modern species and situated outside the Rhinoceros crown-group.

Although statistically limited, our results allow one to draw preliminary considerations on the relation between the shape of the patella and sex attribution among modern rhinoceroses. Our current data do not detect a clear shape distinction between males and females. The appendicular skeleton of modern rhinos is weakly dimorphic (Guérin, 1980; Mallet et al., 2019) with phenotypic dimorphic traits being generally limited to larger horns or slightly heavier males or females (depending on the species) (Dinerstein, 1991, 2011; Zschokke & Baur, 2002). As seen above, body mass variation does not strongly influence the patellar shape in rhinos. Our results suggest that the patella does not bear a significant dimorphic signal among modern rhinos.

Among perissodactyls, the three families (Tapiridae, Equidae, Rhinocerotidae) are distinct, tapirs being very different from both rhinoceroses and equids. This result does not reflect the phylogenetic relationships among the family Perissodactyla, rhinos and tapirs being sister taxa, but rather rely on the shared high development of the medial angle, creating a strong mediolateral asymmetry, absent in tapirs. The patella condition in tapirs is plesiomorphic and thus very close to the one observed in early perissodactyls, although this bone is barely described in literature (Bai et al., 2017), while rhinos and equids show a more derived condition relatively to the supposed basal shape.

Furthermore, intrafamily variations reveal to be higher among rhinos than among equids and tapirs. These relative differences in variation within the three families may be related to their respective evolutionary history. Divergences between the different rhino clades occurred from the Oligocene to Miocene (Fig. 2) (*Bai et al., 2020*; *Antoine et al., 2021*; *Liu et al., 2021*). Tapir branches also diverged during the Miocene (*Steiner & Ryder, 2011*; *MacLaren et al., 2018*) but this clade remained monogeneric, contrary to rhinos. Equids, another monogeneric clade, includes species that diverged very recently during the Pliocene (*Steiner & Ryder, 2011*; *Cirilli et al., 2021*). The deeper ancestry of crown Rhinocerotidae, compared to that of crown Tapiridae and crown Equidae, may explain the higher diversity of patellar shape in this clade relatively to its sister groups.

Microanatomical investigations on the patella of modern perissodactyls revealed no increase in compactness with body mass and no thickening of the cortex on muscle insertions but on the patellar ligament on the cranial side of the bone (*Houssaye, de Perthuis & Houée, 2021*). These results are consistent with ours on the rather conservative nature of this bone in relation to body mass variation. Conversely, the microanatomy distinguishes more rhinos and equids than rhinos and tapirs, contrary to our results, underlining a decoupling between the external morphology of the patella and its internal structure among perissodactyls.

Functional constraints and "knee locking" mechanism

In modern rhinoceroses, our results underline a significant relation between the patellar shape and both its size and the femoral circumference, an excellent proxy of body mass in quadrupeds (*Scott, 1990*; *Campione & Evans, 2012*; *Campione, 2017*). The centroid size of the patella therefore appears directly related to body weight in rhinos, as previously observed for long bones and ankle bones in these animals (*Mallet et al., 2019*; *Etienne et al., 2020b*). However, shape relation with size is limited, allometry accounting for only 12% of the observed shape variation. The influence of body mass on the patellar shape therefore appears as secondary relatively to phylogenetic relationships in rhinos, which partially contradicts our second hypothesis, postulating a stronger effect of mass over phylogeny on the patellar shape. Thus, despite the central functional role of the patella in the knee, and the high stress linked to body mass exerted on this joint, the influence of the weight is much more limited than expected.

Variation linked to size mainly affects the base, the medial angle, and the lateral edge of the patella, as well as the cranial surface. All these areas are insertions for knee extensors, respectively the *m. rectus femoris*, the *m. vastus medialis*, the *m. vastus lateralis* (all three, together with the *m. vastus intermedius*, forming the *m. quadriceps*) and the *m. gluteobiceps* (*Etienne, Houssaye & Hutchinson, 2021*) (Fig. 1). The flattening of the base and the general craniocaudal broadening of the patella in heavy rhino species likely provide more surface area for the insertion of stronger *m. rectus femoris* and *m. gluteobiceps*, while in lighter rhinos the proximal development of the base seems to increase the attachment surface for the *m. vastus lateralis* and *m. vastus medialis* instead. This configuration may reflect that heavy rhinos rely more on central hip muscles, such as the *m. rectus femoris*, to stabilize the knee while lighter rhinos rely on medial and caudal

muscles of the *m. quadriceps*, maybe ensuring more manoeuvrability for this joint. Unfortunately, the scarcity of myological data for lighter rhino species (*Etienne, Houssaye & Hutchinson, 2021*) and the lack of *in vivo* observations prevent us from making further inference between the patellar shape and its relation to attached muscles.

The allometric relation is more strongly marked when considering all perissodactyls (Fig. 9), allometry accounting for 23% of the observed variation. However, body mass alone seems insufficient to explain the shape variation among perissodactyls. A developed medial angle exists both in equids and rhinos but not in tapirs, even though tapirs and equids are in the same range of body mass (hundreds of kilograms), while rhinos can reach several metric tons (Table 1). Medial angle is associated with the presence of a "knee locking" mechanism (*Shockey, 2001*; *Schuurman, Kersten & Weijs, 2003*; *Janis et al., 2012*). Largely studied through the anatomy of the distal femora, this mechanism has barely been considered on the patellar side (*Kappelman, 1988*; *Hermanson & MacFadden, 1996*; *Janis et al., 2012*; *Etienne et al., 2020a*). Our results do confirm the high correspondence between the presence of a developed medial angle on the patella and that of a developed medial trochlear ridge on the femur (*Hermanson & MacFadden, 1996*; *Mallet et al., 2019*). This developed medial angle shared between equids and rhinos therefore appears as convergent in the two clades, implying that this structure may not be totally evolutionary and developmentally homologous in these two clades. Indeed, while the medial angle in equids is extended by a parapatellar cartilage on which the medial patellar ligament attaches (*Hermanson & MacFadden, 1996*: fig. 2), this cartilage seems absent in rhinoceroses (or is little developed–C. Etienne, personal communication), where the bony angle is more extended medially than in equids. As shown in our results, the medial angle in rhinos is more extended and ossified medially compared to equids. This could be directly related to their higher body mass, making cartilage alone insufficient to support the weight of the body and ensure an efficient "knee locking". This would be in line with our second hypothesis, assuming different shapes of patella to ensure an efficient "knee locking" mechanism between equids and rhinos.

Similarly, the craniocaudal development of the base in equids offers a larger surface area for insertions of knee extensors, these muscles being more powerful in equids than in rhinos compared to the respective size of these animals (*Etienne, Houssaye & Hutchinson, 2021*). Myological data lack for tapirs but the reduced surface of the base likely indicates reduced muscle insertions and, therefore, less powerful knee extensors in these animals. Such a craniocaudal development shifts the insertion of the extensor muscles away from the axis of rotation of the knee, thus increasing the moment arm of the joint and the muscular efficiency. This craniocaudal development of the patella in equids likely underlines the extreme cursorial specialization of this clade, while the condition in rhinos appears more as a trade-off between the support of their high body mass, their ability to reach a relatively high speed, and their evolutionary legacy.

The convergent emergence of the knee asymmetry in these clades remain barely understood among ungulates, various authors having supposed a link with either locomotor habit, feeding behaviour or body mass (*Kappelman, 1988*; *Hermanson & MacFadden, 1996*; *Shockey, 2001*; *Shockey et al., 2008*; *Danaher, Shockey & Mihlbachler,*

2009; Janis et al., 2012; Mihlbachler et al., 2014; Etienne et al., 2020a). Locomotor habit shows a marked dichotomy between these clades. Rhinos and equids both practice a transverse gallop while tapirs practice rotatory gallop, involving different limb loadings during the gallop phases (*Economou et al., 2020*). Rotatory gallop involves a phase where both hindlimbs hit the ground, while this never happen in transverse gallop, leading to higher mechanical stress exerted into a single limb in the latter gait. While equids present an extreme cursorial specialization associated with relatively low mass (*Carrano, 1999*), weight-bearing rhinos are still able to reach high speed despite weighting several tons (*Alexander & Pond, 1992; Etienne, Houssaye & Hutchinson, 2021*). An asymmetrical patella could be related to the emergence of a similar gallop in both equids and rhinos, compared to tapirs. Differences in body mass may then explain the further divergences existing in patellar shape between these two clades practicing transverse gallop. Further investigations including a large set of fossil perissodactyls are needed to sharpen the understanding of this puzzling feature and the functional advantages of this presence or absence in ungulates.

CONCLUSION

Our investigation of the shape of the patella among modern rhinoceroses and related extant perissodactyls reveals a higher interspecific than intraspecific morphological variation. Contrary to our predictions, and despite its central functional role in the knee joint and its implication in locomotion, the patella is little affected by variation of body mass between and within species. Rather, the patellar shape follows clear morphotypes existing in each species and even more marked at the scale of the family. This strong shape conservatism may be directly related to its developmental origin, shared with the femur, another bone whose shape has been proved to be highly linked to phylogenetic affinities before functional constraints in perissodactyls. Despite a strong evolutionary legacy leading to a relative shape inertia, the shared presence of a medial angle in rhinos and equids constitutes a clear case of morphological convergence highlighting that functional constraints are also at work on the shape of this sesamoid bone. This asymmetric conformation of the patella is related to a "knee locking" mechanism and maybe to the shared emergence of transverse gallop in both clades. Within this convergence, rhinos present additional shape modifications that may be related to the support of a heavy mass. Further investigations of the shape of the patella among a larger set of extinct Perissodactyla may be helpful for better understanding the morphofunctional evolution of this sesamoid bone in mammals.

ACKNOWLEDGEMENTS

ADDITIONAL INFORMATION AND DECLARATIONS

Funding

Grant Disclosures

Competing Interests

The authors declare that they have no competing interests.

Author Contributions

- Christophe Mallet conceived and designed the experiments, performed the experiments, analyzed the data, prepared figures and/or tables, authored or reviewed drafts of the article, and approved the final draft.
- Alexandra Houssaye conceived and designed the experiments, analyzed the data, authored or reviewed drafts of the article, and approved the final draft.

Data Availability

The following information was supplied regarding data availability:

The R code used to performed the 3D geometric morphometrics are available in the Supplemental File.

The 54 3-D models are available at MorphoSource: https://www.morphosource.org/projects/000366286?locale=en.

The data related to the Institute of Natural Sciences (Belgium) is permanently public, and users can view the media record, but the curators require interested parties to request access to download the data in order to measure the uses made of this investment, prevent any fraudulent or commercial abuses, and allow the curators to measure how these

collections are being used, in order to demonstrate how useful they are to the public and the scientific community, and provide good arguments for further investment in data digitization.

Please contact the curators for download approval: Annelise Folie, Curator of Paleontology Collections, afolie@naturalsciences.be; Olivier S. G. Pauwels, Curator of Recent Vertebrate Collections, opauwels@naturalsciences.be.

Supplemental Information

Supplemental information for this article can be found online at http://dx.doi.org/10.7717/peerj.18067#supplemental-information.

REFERENCES

Abdala V, Vera MC, Ponssa ML. 2017. On the presence of the patella in frogs. *The Anatomical Record* **300(10)**:1747–1755 DOI 10.1002/ar.23629.

Adams DC. 2014. A generalized K statistic for estimating phylogenetic signal from shape and other high-dimensional multivariate data. *Systematic Biology* **63(5)**:685–697 DOI 10.1093/sysbio/syu030.

Adams DC, Otárola-Castillo E. 2013. geomorph: an r package for the collection and analysis of geometric morphometric shape data. *Methods in Ecology and Evolution* **4(4)**:393–399 DOI 10.1111/2041-210X.12035.

Adams DC, Rohlf FJ, Slice DE. 2004. Geometric morphometrics: ten years of progress following the 'revolution'. *Italian Journal of Zoology* **71(1)**:5–16 DOI 10.1080/11250000409356545.

Adler D, Murdoch D. 2020. rgl: 3d visualization device system (OpenGL). *Available at https://cran.r-project.org/web/packages/rgl/index.html*.

Aglietti P, Menchetti PPM. 1995. Biomechanics of the patellofemoral joint. In: Scuderi GR, ed. *The Patella*. New York, NY: Springer, 25–48 DOI 10.1007/978-1-4612-4188-1_3.

Alexander RM, Dimery NJ. 1985. The significance of sesamoids and retro-articular processes for the mechanics of joints. *Journal of Zoology* **205(3)**:357–371 DOI 10.1111/j.1469-7998.1985.tb05622.x.

Alexander RM, Pond CM. 1992. Locomotion and bone strength of the white rhinoceros, *Ceratotherium simum*. *Journal of Zoology* **227(1)**:63–69 DOI 10.1111/j.1469-7998.1992.tb04344.x.

Allen VR, Kambic RE, Gatesy SM, Hutchinson JR. 2017. Gearing effects of the patella (knee extensor muscle sesamoid) of the helmeted guineafowl during terrestrial locomotion. *Journal of Zoology* **303(3)**:178–187 DOI 10.1111/jzo.12485.

Anderson MJ. 2017. Permutational multivariate analysis of variance (PERMANOVA). In: *Wiley StatsRef: Statistics Reference Online*. Hoboken: John Wiley & Sons, Ltd, 1–15 DOI 10.1002/9781118445112.stat07841.

Anderson JF, Hall-Martin A, Russell DA. 1985. Long-bone circumference and weight in mammals, birds and dinosaurs. *Journal of Zoology* **207(1)**:53–61 DOI 10.1111/j.1469-7998.1985.tb04915.x.

Antoine PO, Reyes MC, Amano N, Bautista AP, Chang CH, Claude J, De Vos J, Ingicco T. 2021. A new rhinoceros clade from the Pleistocene of Asia sheds light on mammal dispersals to the Philippines. *Zoological Journal of the Linnean Society* **194(2)**:416–430 DOI 10.1093/zoolinnean/zlab009.

Bai B, Meng J, Wang YQ, Wang HB, Holbrook L. 2017. Osteology of the middle eocene ceratomorph hyrachyus modestus (Mammalia, Perissodactyla). *Bulletin of the American Museum of Natural History* **413**:1–70 DOI 10.1206/0003-0090-413.1.1.

Bai B, Meng J, Zhang C, Gong YX, Wang YQ. 2020. The origin of Rhinocerotoidea and phylogeny of Ceratomorpha (Mammalia, Perissodactyla). *Communications Biology* **3(1)**:1–16 DOI 10.1038/s42003-020-01205-8.

Barone R. 2010a. *Anatomie comparée des mammifères domestiques. Tome 2: Arthrologie et myologie*. Paris: Vigot Frères.

Barone R. 2010b. *Anatomie comparée des mammifères domestiques. Tome 1: Ostéologie*. Paris: Vigot Frères.

Biewener AA, Patek SN. 2018. *Animal locomotion*. New York: Oxford University Press.

Bizarro AH. 1921. On sesamoid and supernumerary bones of the limbs. *Journal of Anatomy* **55**:256–268.

Blanco RE, Gambini R, Fariña RA. 2003. Mechanical model for theoretical determination of maximum running speed in mammals. *Journal of Theoretical Biology* **222(1)**:117–125 DOI 10.1016/S0022-5193(03)00019-5.

Blomberg SP, Garland T, Ives AR, Crespi B. 2003. Testing for phylogenetic signal in comparative data: behavioral traits are more labile. *Evolution* **57**:717–745 DOI 10.1554/0014-3820(2003)057[0717:TFPSIC]2.0.CO;2.

Botton-Divet L. 2017. The form-function relationships in the process of secondary adaptation to an aquatic life. PhD Thesis Thesis. Paris: Université Sorbonne Paris Cité.

Botton-Divet L, Cornette R, Fabre AC, Herrel A, Houssaye A. 2016. Morphological analysis of long bones in semi-aquatic mustelids and their terrestrial relatives. *Integrative and Comparative Biology* **56(6)**:1298–1309 DOI 10.1093/icb/icw124.

Botton-Divet L, Cornette R, Houssaye A, Fabre AC, Herrel A. 2017. Swimming and running: a study of the convergence in long bone morphology among semi-aquatic mustelids (Carnivora: Mustelidae). *Biological Journal of the Linnean Society* **121(1)**:38–49 DOI 10.1093/biolinnean/blw027.

Burchell WJ. 1817. Note sur une nouvelle espèce de Rhinocéros. *Bulletin des Sciences, par la Societe Philomatique de Paris* **1817**:96–97.

Campione NE. 2017. Extrapolating body masses in large terrestrial vertebrates. *Paleobiology* **43(4)**:693–699 DOI 10.1017/pab.2017.9.

Campione NE, Evans DC. 2012. A universal scaling relationship between body mass and proximal limb bone dimensions in quadrupedal terrestrial tetrapods. *BMC Biology* **10**:60 DOI 10.1186/1741-7007-10-60.

Carrano MT. 1999. What, if anything, is a cursor? Categories versus continua for determining locomotor habit in mammals and dinosaurs. *Journal of Zoology* **247(1)**:29–42 DOI 10.1111/j.1469-7998.1999.tb00190.x.

Chadwick KP, Regnault S, Allen V, Hutchinson JR. 2014. Three-dimensional anatomy of the ostrich (Struthio camelus) knee joint. *PeerJ* **2(1)**:e706 DOI 10.7717/peerj.706.

Cignoni P, Callieri M, Corsini M, Dellepiane M, Ganovelli F, Ranzuglia G. 2008. MeshLab: an open-source mesh processing tool. In: *Eurographics Italian Chapter Conference.* Vol. 2008. Eindhoven: The Eurographics Association, 129–136 DOI 10.2312/LocalChapterEvents/ItalChap/ItalianChapConf2008/129-136.

Cirilli O, Pandolfi L, Rook L, Bernor RL. 2021. Evolution of Old World Equus and origin of the zebra-ass clade. *Scientific Reports* **11(1)**:10156 DOI 10.1038/s41598-021-89440-9.

Corina Vera M, Laura Ponssa M, Abdala V. 2015. Further data on sesamoid identity from two anuran species. *The Anatomical Record* **298(8)**:1376–1394 DOI 10.1002/ar.23158.

Costa-Pereira R, Araújo MS, Paiva F, Tavares LER. 2016. Functional morphology of the tetra fish Astyanax lacustris differs between divergent habitats in the Pantanal wetlands. *Journal of Fish Biology* **89(2)**:1450–1458 DOI 10.1111/jfb.13026.

Damuth JD, MacFadden BJ. 1990. *Body size in mammalian paleobiology: estimation and biological implications*. Cambridge: Cambridge University Press.

Dan M, Parr W, Broe D, Cross M, Walsh WR. 2018. Biomechanics of the knee extensor mechanism and its relationship to patella tendinopathy: a review. *Journal of Orthopaedic Research* **36(12)**:3105–3112 DOI 10.1002/jor.24120.

Danaher K, Shockey BJ, Mihlbachler MC. 2009. Perissodactyl patella: morphological variation and phylogenetic signifiance in a neglected element. *Journal of Vertebrate Paleontology* **29**:85A DOI 10.1080/02724634.2009.10411818.

Dinerstein E. 1991. Sexual dimorphism in the greater one-horned rhinoceros (Rhinoceros unicornis). *Journal of Mammalogy* **72(3)**:450–457 DOI 10.2307/1382127.

Dinerstein E. 2011. Family rhinocerotidae (Rhinoceroses). In: Wilson DE, Mittermeier RA, eds. *Handbook of the Mammals of the World*. Barcelona: Don E. Wilson & Russel A. Mittermeier, 144–181.

Dixon P. 2003. VEGAN, a package of R functions for community ecology. *Journal of Vegetation Science* **14(6)**:927–930 DOI 10.1111/j.1654-1103.2003.tb02228.x.

Economou G, McGrath M, Wajsberg J, Granatosky MC. 2020. Perissodactyla locomotion. In: Vonk J, Shackelford T, eds. *Encyclopedia of Animal Cognition and Behavior*. Cham: Springer International Publishing, 1–8 DOI 10.1007/978-3-319-47829-6_887-1.

Eisenmann V, Guérin C. 1984. Morphologie fonctionnelle et environnement chez les périssodactyles. *Geobios* **17(6)**:69–74 DOI 10.1016/S0016-6995(84)80158-8.

Ellis MI, Seedhom BB, Wright V, Dowson D. 1980. An evaluation of the ratio between the tensions along the quadriceps tendon and the patellar ligament. *Engineering in Medicine* **9(4)**:189–194 DOI 10.1243/EMED_JOUR_1980_009_049_02.

Etienne C, Filippo A, Cornette R, Houssaye A. 2020a. Effect of mass and habitat on the shape of limb long bones: a morpho-functional investigation on Bovidae (Mammalia: Cetartiodactyla). *Journal of Anatomy* **238(4)**:886–904 DOI 10.1111/joa.13359.

Etienne C, Houssaye A, Hutchinson JR. 2021. Limb myology and muscle architecture of the Indian rhinoceros Rhinoceros unicornis and the white rhinoceros Ceratotherium simum (Mammalia: Rhinocerotidae). *PeerJ* **9(4)**:e11314 DOI 10.7717/peerj.11314.

Etienne C, Mallet C, Cornette R, Houssaye A. 2020b. Influence of mass on tarsus shape variation: a morphometrical investigation among Rhinocerotidae (Mammalia: Perissodactyla). *Biological Journal of the Linnean Society* **129(4)**:950–974 DOI 10.1093/biolinnean/blaa005.

Eyal S, Blitz E, Shwartz Y, Akiyama H, Schweitzer R, Zelzer E. 2015. On the development of the patella. *Development* **142(10)**:1831–1839 DOI 10.1242/dev.121970.

Eyal S, Rubin S, Krief S, Levin L, Zelzer E. 2019. Common cellular origin and diverging developmental programs for different sesamoid bones. *Development* **146(4)**:dev167452 DOI 10.1242/dev.167452.

Fabre A-C, Cornette R, Peigné S, Goswami A. 2013. Influence of body mass on the shape of forelimb in musteloid carnivorans. *Biological Journal of the Linnean Society* **110(1)**:91–103 DOI 10.1111/bij.12103.

Federative Committee on Anatomical Terminology. 1998. *Terminologia anatomica.* Stuttgart: Georg Thieme Verlag.

Fischer G. 1814. *Zoognosia: tabulis synopticis illustrata.* Vol. 3. Moscow: Typis Nicolai Sergeidis Vsevolozsky, 732 DOI 10.5962/bhl.title.42225.

Garland T. 1983. The relation between maximal running speed and body mass in terrestrial mammals. *Journal of Zoology* **199(2)**:157–170 DOI 10.1111/j.1469-7998.1983.tb02087.x.

Garnoeva R. 2022. Patellar morphology in small breed dogs with medial patellar luxation. *Egyptian Journal of Veterinary Sciences* **53(3)**:403–408 DOI 10.21608/ejvs.2022.121266.1327.

Goodall C. 1991. Procrustes methods in the statistical analysis of shape. *Journal of the Royal Statistical Society: Series B (Methodological)* **53(2)**:285–321 DOI 10.1111/j.2517-6161.1991.tb01825.x.

Gould SJ. 2002. *The structure of evolutionary theory.* Cambridge, London: Harvard University Press.

Gower JC. 1975. Generalized procrustes analysis. *Psychometrika* **40(1)**:33–51 DOI 10.1007/BF02291478.

Guérin C. 1980. Les Rhinocéros (Mammalia, Perissodactyla) du Miocène terminal au Pléistocène supérieur en Europe occidentale. Comparaison avec les espèces actuelles. *Documents du Laboratoire de Geologie de la Faculte des Sciences de Lyon* **79**:3–1183.

Gunz P, Mitteroecker P. 2013. Semilandmarks: a method for quantifying curves and surfaces. *Hystrix, the Italian Journal of Mammalogy* **24**:103–109 DOI 10.4404/hystrix-24.1-6292.

Gunz P, Mitteroecker P, Bookstein FL. 2005. Semilandmarks in three dimensions. In: Slice DE, ed. *Modern Morphometrics in Physical Anthropology. Developments in Primatology: Progress and Prospects.* New York: Springer, 73–98 DOI 10.1007/0-387-27614-9_3.

Hall BK. 2007. *Fins into limbs: evolution, development, and transformation.* Chicago: University of Chicago Press.

Hallgrímsson B, Jamniczky H, Young NM, Rolian C, Parsons TE, Boughner JC, Marcucio RS. 2009. Deciphering the palimpsest: studying the relationship between morphological integration and phenotypic covariation. *Evolutionary Biology* **36(4)**:355–376 DOI 10.1007/s11692-009-9076-5.

Hanot P, Herrel A, Guintard C, Cornette R. 2017. Morphological integration in the appendicular skeleton of two domestic taxa: the horse and donkey. *Proceedings of the Royal Society B: Biological Sciences* **284(1864)**:20171241 DOI 10.1098/rspb.2017.1241.

Hanot P, Herrel A, Guintard C, Cornette R. 2018. The impact of artificial selection on morphological integration in the appendicular skeleton of domestic horses. *Journal of Anatomy* **232(4)**:657–673 DOI 10.1111/joa.12772.

Hermanson JW, MacFadden BJ. 1996. Evolutionary and functional morphology of the knee in fossil and extant horses (Equidae). *Journal of Vertebrate Paleontology* **16(2)**:349–357 DOI 10.1080/02724634.1996.10011321.

Hildebrand M. 1974. *Analysis of vertebrate structure.* New York: John Wiley & Sons.

Ho J, Tumkaya T, Aryal S, Choi H, Claridge-Chang A. 2019. Moving beyond P values: data analysis with estimation graphics. *Nature Methods* **16(7)**:565–566 DOI 10.1038/s41592-019-0470-3.

Houssaye A, de Perthuis A, Houée G. 2021. Sesamoid bones also show functional adaptation in their microanatomy—the example of the patella in Perissodactyla. *Journal of Anatomy* **240(1)**:50–65 DOI 10.1111/joa.13530.

Janis CM, Shoshitaishvili B, Kambic R, Figueirido B. 2012. On their knees: distal femur asymmetry in ungulates and its relationship to body size and locomotion. *Journal of Vertebrate Paleontology* **32(2)**:433–445 DOI 10.1080/02724634.2012.635737.

Jerez A, Mangione S, Abdala V. 2010. Occurrence and distribution of sesamoid bones in squamates: a comparative approach. *Acta Zoologica* **91(3)**:295–305 DOI 10.1111/j.1463-6395.2009.00408.x.

Kappelman J. 1988. Morphology and locomotor adaptations of the bovid femur in relation to habitat. *Journal of Morphology* **198(1)**:119–130 DOI 10.1002/jmor.1051980111.

Klingenberg CP. 2016. Size, shape, and form: concepts of allometry in geometric morphometrics. *Development Genes and Evolution* **226(3)**:113–137 DOI 10.1007/s00427-016-0539-2.

Liu S, Westbury MV, Dussex N, Mitchell KJ, Sinding MHS, Heintzman PD, Duchêne DA, Kapp JD, von Seth J, Heiniger H, Sánchez-Barreiro F, Margaryan A, André-Olsen R, Cahsan BD, Meng G, Yang C, Chen L, van der Valk T, Moodley Y, Rookmaaker K, Bruford MW, Ryder O, Steiner C, Sonsbeek LGRB, Vartanyan S, Guo C, Cooper A, Kosintsev P, Kirillova I, Lister AM, Marques-Bonet T, Gopalakrishnan S, Dunn RR, Lorenzen ED, Shapiro B, Zhang G, Antoine PO, Dalén L, Gilbert MTP. 2021. Ancient and modern genomes unravel the evolutionary history of the rhinoceros family. *Cell* **184(19)**:4874–4885.e16 DOI 10.1016/j.cell.2021.07.032.

Lovejoy CO. 2007. The natural history of human gait and posture: Part 3. The knee. *Gait & Posture* **25(3)**:325–341 DOI 10.1016/j.gaitpost.2006.05.001.

MacLaren JA, Hulbert RC Jr, Wallace SC, Nauwelaerts S. 2018. A morphometric analysis of the forelimb in the genus Tapirus (Perissodactyla: Tapiridae) reveals influences of habitat, phylogeny and size through time and across geographical space. *Zoological Journal of the Linnean Society* **20(2)**:1–17 DOI 10.1093/zoolinnean/zly019.

MacLaren JA, Nauwelaerts S. 2016. A three-dimensional morphometric analysis of upper forelimb morphology in the enigmatic tapir (Perissodactyla: Tapirus) hints at subtle variations in locomotor ecology. *Journal of Morphology* **277(11)**:1469–1485 DOI 10.1002/jmor.20588.

MacLaren JA, Nauwelaerts S. 2017. Interspecific variation in the tetradactyl manus of modern tapirs (Perissodactyla: Tapirus) exposed using geometric morphometrics. *Journal of Morphology* **278(11)**:1517–1535 DOI 10.1002/jmor.20728.

Mallet C, Billet G, Cornette R, Alexandra Houssaye A. 2022. Adaptation to graviportality in Rhinocerotoidea? An investigation through the long bone shape variation in their hindlimb. *Zoological Journal of the Linnean Society* **196(3)**:1235–1271 DOI 10.1093/zoolinnean/zlac007.

Mallet C, Billet G, Houssaye A, Cornette R. 2020. A first glimpse at the influence of body mass in the morphological integration of the limb long bones: an investigation in modern rhinoceroses. *Journal of Anatomy* **237(4)**:704–726 DOI 10.1111/joa.13232.

Mallet C, Cornette R, Billet G, Houssaye A. 2019. Interspecific variation in the limb long bones among modern rhinoceroses—extent and drivers. *PeerJ* **7(5)**:e7647 DOI 10.7717/peerj.7647.

Mallet C, Houssaye A, Cornette R, Billet G. 2021. Long bone shape variation in the forelimb of Rhinocerotoidea—relation with size, body mass and body proportions. *Zoological Journal of the Linnean Society* **196(3)**:1201–1234 DOI 10.1093/zoolinnean/zlab095.

Medici EP. 2011. Family Tapiridae (Tapirs). In: Wilson DE, Mittermeier RA, eds. *Handbook of the Mammals of the World*. Barcelona: Lynx Edicions, 182–203.

Mihlbachler MC, Lau T, Kapner D, Shockey BJ. 2014. Coevolution of the shoulder and knee in Ungulates: implications of the evolution of locomotion and standing. *Available at https://vertpaleo.org/wp-content/uploads/2021/04/SVP-2014-Program-and-Abstract-Book-10-14-2014.pdf*.

Mitteroecker P, Gunz P, Windhager S, Schaefer K. 2013. A brief review of shape, form, and allometry in geometric morphometrics, with applications to human facial morphology. *Hystrix, the Italian Journal of Mammalogy* **24**:59–66 DOI 10.4404/hystrix-24.1-6369.

Mitteroecker P, Schaefer K. 2022. Thirty years of geometric morphometrics: achievements, challenges, and the ongoing quest for biological meaningfulness. *American Journal of Biological Anthropology* **178(S74)**:181–210 DOI 10.1002/ajpa.24531.

Pandolfi L, Antoine PO, Bukhsianidze M, Lordkipanidze D, Rook L. 2021. Northern Eurasian rhinocerotines (Mammalia, Perissodactyla) by the Pliocene-Pleistocene transition: phylogeny and historical biogeography. *Journal of Systematic Palaeontology* **19(15)**:1–27 DOI 10.1080/14772019.2021.1995907.

Pina M, DeMiguel D, Puigvert F, Marcé-Nogué J, Moyà-Solà S. 2020. Knee function through finite element analysis and the role of Miocene hominoids in our understanding of the origin of antipronograde behaviours: the Pierolapithecus catalaunicus patella as a case study. *Palaeontology* **63(3)**:459–475 DOI 10.1111/pala.12466.

Pintore R, Houssaye A, Nesbitt SJ, Hutchinson JR. 2021. Femoral specializations to locomotor habits in early archosauriforms. *Journal of Anatomy* **240(5)**:867–892 DOI 10.1111/joa.13598.

Polly PD. 2007. Limbs in mammalian evolution. Chapter 15. In: Hall BK, ed. *Fins into Limbs: Evolution, Development, and Transformation*. Chicago: University of Chicago Press, 245–268.

Ponssa ML, Goldberg J, Abdala V. 2010. Sesamoids in anurans: new data, old issues. *The Anatomical Record* **293(10)**:1646–1668 DOI 10.1002/ar.21212.

R Core Team. 2014. *R: a language and environment for statistical computing.* Vienna: R Foundation for Statistical Computing. *Available at* https://www.r-project.org.

Raux P, Townsend PR, Miegel R, Rose RM, Radin EL. 1975. Trabecular architecture of the human patella. *Journal of Biomechanics* **8(1)**:1–7 DOI 10.1016/0021-9290(75)90037-8.

Raymond KR, Prothero DR. 2012. Comparative variability of intermembranous and endochondral bones in Pleistocene mammals. *Palaeontologia Electronica* **13**:14.

Revell LJ. 2012. phytools: an R package for phylogenetic comparative biology (and other things). *Methods in Ecology and Evolution* **3(2)**:217–223 DOI 10.1111/j.2041-210X.2011.00169.x.

Rohlf FJ, Slice D. 1990. Extensions of the procrustes method for the optimal superimposition of landmarks. *Systematic Biology* **39(1)**:40–59 DOI 10.2307/2992207.

Rubenstein DI. 2011. Family Equidae (Horses and relatives). In: Wilson DE, Mittermeier RA, eds. *Handbook of the Mammals of the World*. Barcelona: Lynx Edicions, 106–143.

Samuels ME, Regnault S, Hutchinson JR. 2017. Evolution of the patellar sesamoid bone in mammals. *PeerJ* **5(7055)**:e3103 DOI 10.7717/peerj.3103.

Schlager S. 2017. Chapter 9—morpho and Rvcg—shape analysis in R: R-packages for geometric morphometrics, shape analysis and surface manipulations. In: Zheng G, Li S, Székely G, eds. *Statistical Shape and Deformation Analysis*. Cambridge: Academic Press, 217–256 DOI 10.1016/B978-0-12-810493-4.00011-0.

Schneider MTY, Rooks N, Besier T. 2022. Cartilage thickness and bone shape variations as a function of sex, height, body mass, and age in young adult knees. *Scientific Reports* **12(1)**:11707 DOI 10.1038/s41598-022-15585-w.

Schuurman SO, Kersten W, Weijs WA. 2003. The equine hind limb is actively stabilized during standing. *Journal of Anatomy* **202(4)**:355–362 DOI 10.1046/j.1469-7580.2003.00166.x.

Scott KM. 1990. Postcranial dimensions of ungulates as predictors of body mass. In: Damuth JD, MacFadden BJ, eds. *Body Size in Mammalian Palaeobiology: Estimation and Biological Implications*. Cambridge: Cambridge University Press, 301–335.

Seilacher A. 1970. Arbeitskonzept zur konstruktions-morphologie. *Lethaia* **3(4)**:393–396 DOI 10.1111/j.1502-3931.1970.tb00830.x.

Seilacher A. 1991. Self-organizing mechanisms in morphogenesis and evolution. In: Schmidt-Kittler N, Vogel K, eds. *Constructional Morphology and Evolution*. Berlin, Heidelberg: Springer, 251–271 DOI 10.1007/978-3-642-76156-0_17.

Serio C, Raia P, Meloro C. 2020. Locomotory adaptations in 3D humerus geometry of xenarthra: testing for convergence. *Frontiers in Ecology and Evolution* **8**:166 DOI 10.3389/fevo.2020.00139.

Shockey BJ. 2001. Specialized knee joints in some extinct, endemic, South American herbivores. *Acta Palaeontologica Polonica* **46**:277–288.

Shockey BJ, Mihlbachler MC, Solounias N, Hayes BP. 2008. Functional morphology of the knee in rhinos and the evolution of knee locking mechanisms among rhinocerotoid perissodactyls. *Journal of Vertebrate Paleontology* **28**:142A DOI 10.1080/02724634.2008.10010459.

Steiner CC, Ryder OA. 2011. Molecular phylogeny and evolution of the Perissodactyla. *Zoological Journal of the Linnean Society* **163(4)**:1289–1303 DOI 10.1111/j.1096-3642.2011.00752.x.

Toumi H, Higashiyama I, Suzuki D, Kumai T, Bydder G, McGonagle D, Emery P, Fairclough J, Benjamin M. 2006. Regional variations in human patellar trabecular architecture and the structure of the proximal patellar tendon enthesis. *Journal of Anatomy* **208(1)**:47–57 DOI 10.1111/j.1469-7580.2006.00501.x.

Valois H. 1917. La valeur morphologique de la rotule chez les mammifères. *Bulletins et Mémoires de la Société d'Anthropologie de Paris* **8(1)**:1–34 DOI 10.3406/bmsap.1917.8819.

Vickaryous MK, Olson WM. 2008. Sesamoids and ossicles in the appendicular skeleton. In: Hall BK, ed. *Fins into Limbs: Evolution, Development, and Transformation*. Chicago: University of Chicago Press, 323–341.

Wasserstein RL, Schirm AL, Lazar NA. 2019. Moving to a world beyond "p < 0.05". *The American Statistician* **73(sup1)**:1–19 DOI 10.1080/00031305.2019.1583913.

Wiley DF, Amenta N, Alcantara DA, Ghosh D, Kil YJ, Delson E, Harcourt-Smith W, Rohlf FJ, John STK, Hamann B. 2005. Evolutionary morphing. In: *Proceedings of IEEE Visualization 2005*. Piscataway: IEEE.

Zelditch ML, Swiderski DL, Sheets HD, Fink WL. 2012. *Geometric morphometrics for biologists: a primer*. Cambridge, MA: Academic Press.

Zschokke S, Baur B. 2002. Inbreeding, outbreeding, infant growth, and size dimorphism in captive Indian rhinoceros (*Rhinoceros unicornis*). *Canadian Journal of Zoology* **80(11)**:2014–2023 DOI 10.1139/z02-183.